Natural variation of diterpenoid phytoalexin production in *Oryza sativa*

（イネにおけるジテルペノイドファイトアレキシン生産の種内多様性に関する研究）

假谷　佳祐

Keisuke Kariya

2024

Contents

Chapter 1
General introduction

Every plant species accumulates diverse and characteristic specialized metabolites, with the estimated number of specialized metabolites produced by plants being 200,000–1 million (Wang *et al.*, 2019). Some of these metabolites are universally distributed within the plant kingdom, whereas others are species-specific. As plants cannot select the environment in which they grow, their accumulation of various specialized metabolites is considered a crucial survival strategy for adapting to their habitat. The specialized metabolites that accumulate in plants are classified as terpenoids, flavonoids, benzenoids, phenylpropanoids, nitrogen-containing compounds, etc., based on their chemical structures (Wang *et al.*, 2019). These metabolites exhibit diverse bioactivities, including antimicrobial activities, attractant or repellent activities on other organisms, and promoting or inhibitory activities for the growth and development of plants (Jain *et al.*, 2018).

The compositions of specialized metabolites among the cultivars or strains within a species exhibit variations. For example, in *Artemisia annua* L., high- and low-artemisinin-producing chemotypes have been characterized (Czechowski et al., 2018). The chemotype differences were caused by the gene expression level of *DBR2* (artemisinic aldehyde $\Delta^{11(13)}$ reductase), which was lower in low-artemesinin-producing chemotypes. Similarly, the diploid wheat species *Triticum boeoticum* Boiss. shows benzoxazinone-accumulating and non-benzoxazinone-accumulating chemotypes. The non-benzoxazinone-accumulating chemotype was shown to be caused by a transversion at the *Bx1* gene that encodes the first committed enzyme in the benzoxazinone

biosynthetic pathway (Nomura et al., 2007). Kliebenstein *et al.* (2001) quantitatively analyzed 34 glucosinolates in the leaves and seeds of 39 ecotypes of *Arabidopsis thaliana* (L.) Heynh. and demonstrated the existence of natural variation in the composition of glucosinolates. The differences in the amount of accumulated glucosinolates among the ecotypes ranged from 2.5- to 1220-fold (except when the values were below the limit of detection). In *A. thaliana*, the side chain length is one of the factors that contribute to the structural diversity of glucosinolates and is mechanistically determined by alleles at the *GS-ELONG* locus (Kroymann et al., 2003). It has been suggested that geographic patterns in *GS-ELONG* are strongly correlated with changes in the relative abundance of two specialist aphids (Zust et al., 2012). Factors that may cause intraspecific diversity in the accumulation of secondary metabolites include 1) adaptation to biotic and abiotic stresses, 2) population dynamics, such as the formation of population structure and changes in population size, or 3) the fact that diversity in secondary metabolites is not caused by natural selection (neutral). Therefore, studying natural variation provide insight not only into changes in secondary metabolites or metabolic pathway, but also into the adaptation to habitat and evolutionary trajectory in terms of secondary metabolites.

Plants have various defense mechanisms against pathogens, which are classified into physical and chemical defenses. Physical defenses include the accumulation of phenolic polymers in cell walls in response to pathogens and the presence of a cuticle layer on the surface of leaves. Chemical defenses include the accumulation of antimicrobial enzymes and specialized toxic metabolites including phytoalexins. Phytoalexins have been found in numerous plant species after pisatin was first identified in peas (*Pisum sativum* L.) (Perrin and Bottomley, 1962). Poaceae species are not an exception; the representative phytoalexins in Poaceae species are avenanthramides in oats

(*Avena sativa* L.) (Mayama *et al*., 1982; Miyagawa *et al*., 1995), kauralexins and zealexins in maize (*Zea mays* L.) (Schmelz *et al*., 2011; Huffaker *et al*., 2011), and a serotonin dimer in barley (*Hordeum vulgare* L.) (Ishihara *et al*., 2017). Phytoalexins are biosynthesized by various pathways, being classified into terpenoids, flavonoids, alkaloids, and compounds derived from multiple biosynthetic pathways.

The phytoalexins identified in rice (*Oryza sativa* L.) (Figure 1.1) include the flavonoid phytoalexin sakuranetin (Kodama *et al*., 1992a), the diterpenoid phytoalexins oryzalexins A–F and S (Akatsuka *et al*., 1983, 1985; Kono *et al*., 1984; Sekido *et al*., 1986; Kato *et al*., 1993, 1994; Kodama *et al*., 1992b), phytocassanes A–F (Koga *et al*., 1995, 1997; Horie *et al*., 2015), momilactones A and B (Cartwright *et al*., 1981), and *ent*-

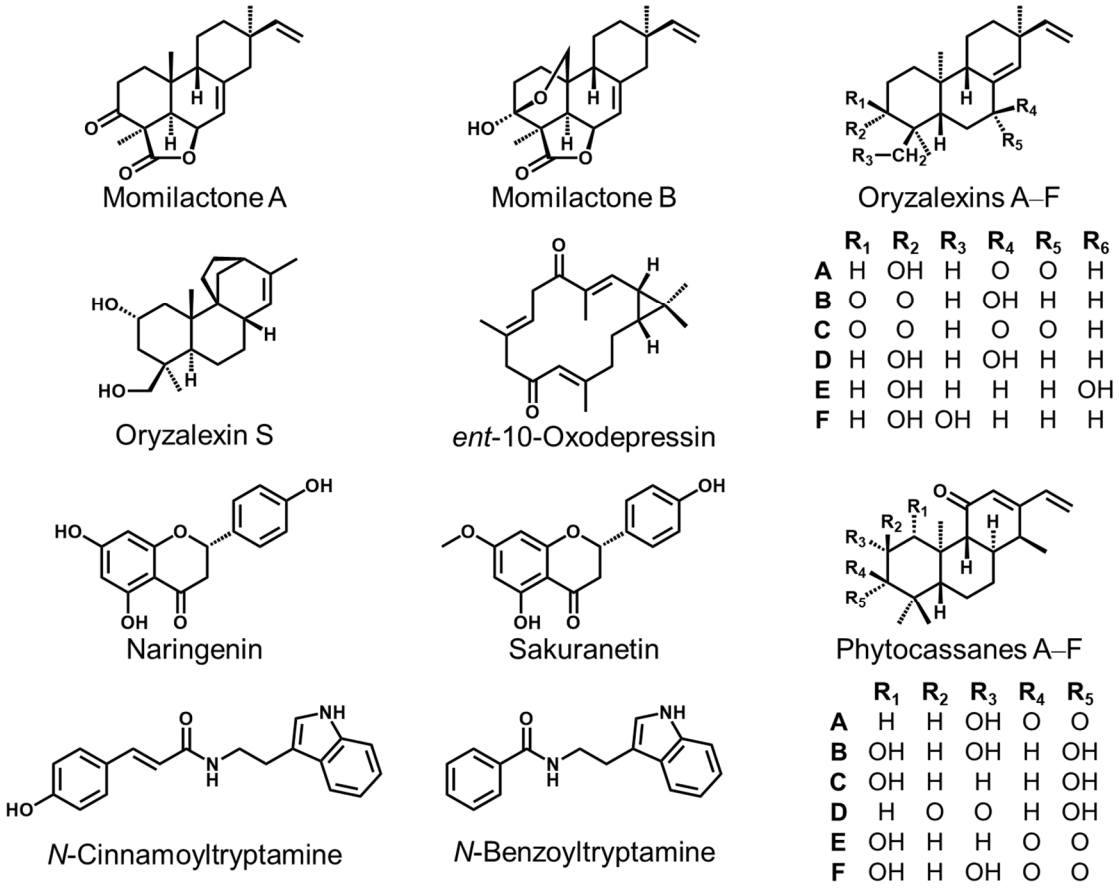

	R_1	R_2	R_3	R_4	R_5	R_6
A	H	OH	H	O	O	H
B	O	O	H	OH	H	H
C	O	O	H	O	O	H
D	H	OH	H	OH	H	H
E	H	OH	H	H	H	OH
F	H	OH	OH	H	H	H

	R_1	R_2	R_3	R_4	R_5
A	H	H	OH	O	O
B	OH	H	OH	H	OH
C	OH	H	H	H	OH
D	H	O	O	H	OH
E	OH	H	H	O	O
F	OH	H	OH	O	O

Figure 1.1. Phytoalexins in rice.

10-oxodepressin (Inoue *et al*., 2013). In addition, phenylamides, such as *N*-cinnamoyltryptamine and *N*-benzoyltryptamine, serves as phytoalexins (Morimoto *et al*., 2018). This wide array of compounds represents multiple layers in the chemical defense system. Phytoalexin production can be induced by pathogen infection, irradiation by UV light, or treatment with elicitors such as *N*-acetylchitooligosaccharides, jasmonic acid (JA), and copper chloride (Akagi *et al*., 2014).

The presence of multiple genes encoding for diterpene cyclases enables rice plants to biosynthesize diverse diterpenoids with distinct carbon skeletons (Figure 1.2). Tricyclic diterpenes are biosynthesized by copalyl diphosphate (CDP) synthase (CPS) and kaurene synthase-like (KSL) from geranylgeranyl pyrophosphate (GGPP). The rice genome contains four CPSs and 11 KSLs, and their functions have been analyzed. CPS2 and CPS4 contribute to the production of phytoalexins by catalyzing the conversions of GGPP into *ent*-CDP and *syn*-CDP, respectively; both products exhibit different steric configurations (Otomo *et al*., 2004). Among the *KSL*s, *KSL3* and *KSL9* are pseudogenes (Xu *et al*., 2007; Sakamoto *et al*., 2004), and the products of the remaining nine *KSLs* differ (Toyomasu *et al*., 2020). Four of these genes, *KSL4*, *KSL7*, *KSL8*, and *KSL10*, are involved in the biosynthesis of phytoalexins. *KSL8* and *KSL10* contain two alleles, which encode the enzymes that catalyze distinct reactions (Toyomasu *et al*., 2016).

Gene manipulation techniques have the enabled examination of the roles of phytoalexins in the rejection of pathogenic infection. Diterpenoid phytoalexins have been demonstrated to contribute to resistance to rice blast fungus [*Pyricularia oryzae* (syn. *Magnaporthe oryzae*)] (Toyomasu *et al*., 2014), a strain of *Magnaporthe poae* isolated from wheat (Lu *et al*., 2018), and bacterial pathogen *Xanthomonas oryzae* pv. *oryzae* (Ishiyama) Dye (Lu *et al*., 2018; Zhang *et al*., 2021; Li *et al*., 2022) by knocking out or

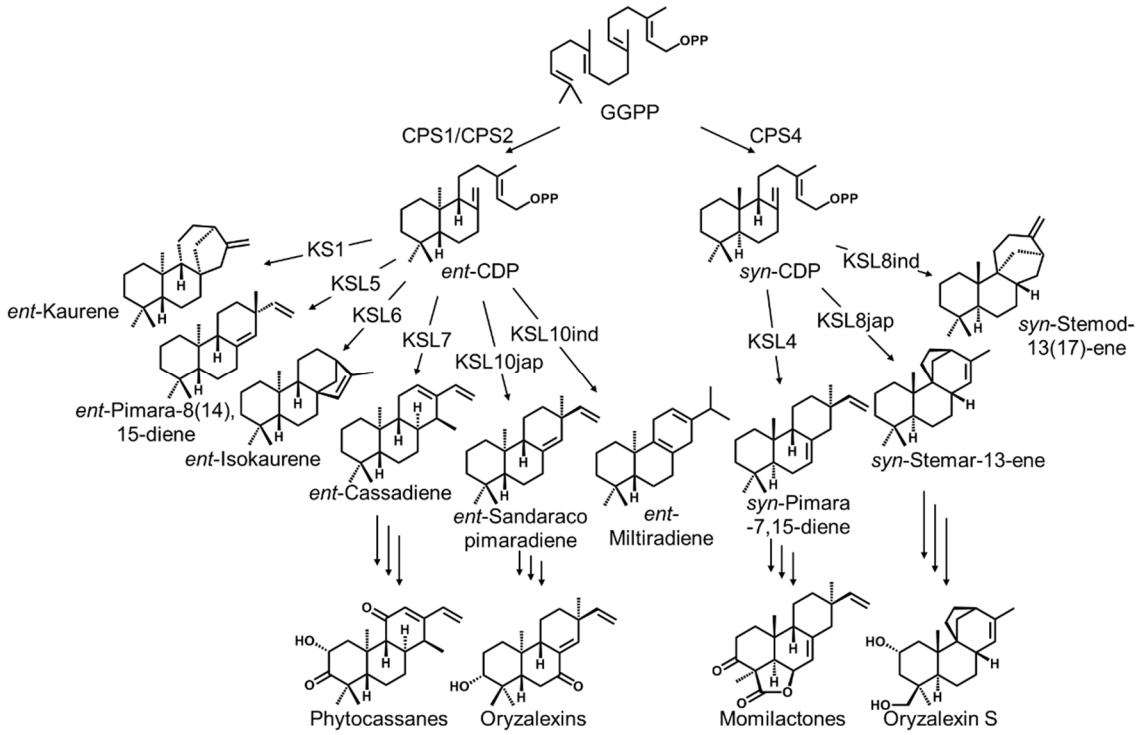

Figure 1.2. Biosynthetic pathways of rice diterpenoid phytoalexins.

knocking down of biosynthetic genes. In addition to the interactions with microorganisms, diterpenoid phytoalexins demonstrate pleiotropic functions such as resistance against nematode (Desmedt *et al*., 2022) and allelopathy against weeds (Kato-Noguchi, 2004). Thus, these compounds are essential tools allowing rice plants to control the surrounding organisms.

The number of rice cultivars in the world is estimated to be 100,000–120,000 (Vaughan, 1991), and now approximately 780,000 accessions, majority of which are landraces and old cultivars, are available from various gene banks (FAO, 2010). It is thus reasonable to assume that this species contains a large amount of intraspecies diversity in diterpenoid phytoalexin production. Diversity is thought to reflect the processes of natural and artificial selection. Studying natural variation may thus reveal what traits were acquired for the lineage in a species to adapt to their habitat. Therefore, an examination

of the natural variation of rice diterpenoid phytoalexins provides an interesting viewpoint of the evolution of the defense-related specialized metabolism in rice. In this study, diterpenoid phytoalexin contents were analyzed in various cultivars (chapter 2). During the analysis, two compounds that were presumed to be unreported diterpenoids were found and identified (chapter 2). In addition, some cultivars were found to accumulate very low levels of diterpenoid phytoalexins. In particular, 'Jinguoyin', a cultivar from China, did not accumulate any of analyzed diterpenoid phytoalexins at detectable levels. Because phytoalexins play a crucial role in disease resistance, it is presumed that this cultivar accumulates different phytoalexins in response to pathogen attack. Therefore, phytoalexins were explored in the cultivar 'Jinguoyin' (chapter 3).

Chapter 2
Intraspecific diversity of diterpenoid phytoalexin accumulation in cultivated and wild rice

2-1 Introduction

Plants accumulate various secondary metabolites to adapt to their habitat. Even within the same species, the composition of secondary metabolites varies by habitat or population. Such diversity within a specie could have resulted from natural selection or from artificial selection. Therefore, studying natural variation may thus reveal what traits were acquired for the lineage in a species to adapt to their environment.

The intraspecific diversity of flavonoid phytoalexins accumulation has been revealed (Murata *et al*., 2020) by investigation of World Rice Core Collection (WRC), a suitable material for investigating the natural variation of various rice traits (Kojima *et al*., 2005). WRC comprises 69 accessions, retaining 90% of the restriction fragment length polymorphism alleles detected in ~300 accessions that were selected based on the passport data from the entire rice collection (~30,000 accessions) maintained at the National Agriculture and Food Research Organization (NARO) in Japan. In JA-treated leaves, some of the cultivars accumulated sakuranetin, whereas the others accumulated naringenin, which is the immediate precursor of sakuranetin (Murata *et al*., 2020).

It was presumed that there is natural variation in diterpenoid phytoalexin production in rice. Therefore, quantitative analyses were performed for five diterpenoid phytoalexins, oryzalexin A, momilactones A and B, and phytocassanes A and D, using WRC cultivars. In addition, phytoalexins in wild relatives of *O. sativa* were analyzed to obtain insight into the evolution of phytoalexin biosynthesis in rice. During the analysis,

two unknown compounds, which were presumed to be an isomer of momilactone A, were detected. To reveal the natural variation of phytoalexin production in rice, these compounds were isolated and subjected to the spectroscopic analysis for the determination of their chemical structures.

2-2 Results

Accumulation of oryzalexin A, momilactones A and B, and phytocassanes A and D in various rice cultivars and wild rice species

The accumulation of the representative rice diterpenoid phytoalexins, oryzalexin A, momilactones A and B, and phytocassanes A and D were analyzed in cultivars from the World Rice Core Collection (WRC), which covers a wide range of genetic diversity of rice (Kojima *et al*., 2005). The leaves of rice seedlings were irradiated with UV light for 10 min, and the metabolites were extracted and analyzed after 72 h incubation.

Oryzalexin A were detected in 12 of 69 cultivars, and only six cultivars accumulated oryzalexin A at concentrations higher than 10 nmol g^{-1} FW (Figure 2.1a). The maximum amount of oryzalexin A was 79.4 nmol g^{-1} FW in 'Phulba' (WRC67). Oryzalexin A was found in both *japonica* (6 cultivars) and *indica* (4 cultivars), and the geographic distribution of oryzalexin-containing cultivars was not biased.

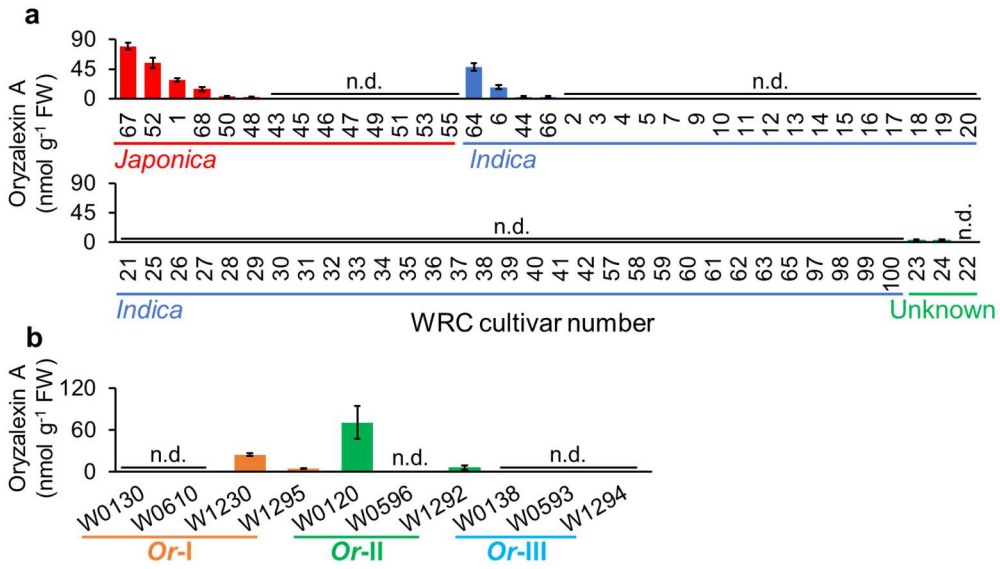

Figure 2.1. Accumulation of oryzalexin A in cultivars in world rice core collection (**a**) and *O. rufipogon* strains (**b**) after UV light irradiation. Values are means ± SD of three biological replicates. Different letters indicate significant differences ($p<0.05$; Tukey-Kramer method).

The analysis was expanded to the wild rice species *O. rufipogon* because this specie is considered a progenitor of cultivated rice. *O. rufipogon* strains are classified into three clades, *Or*-I, *Or*-II, or *Or*-III, based on genetic analysis (Huang *et al*., 2012). *Or*-I and *Or*-III is phylogenetically close to the indica and japonica subspecies in *O. sativa*, respectively, and *Or*-II is a clade located between *Or*-I and *Or*-III in phylogenetic analysis (Huang *et al*., 2012). We selected several strains in each clade and analyzed the accumulation of oryzalexin A in leaves irradiated by UV light. As shown in Figure 2.1b, four strains in *Or*-I and *Or*-II, but none in *Or*-III, accumulated oryzalexin A.

Momilactone A was detected in 64 out of 69 cultivars (Figure 2.2a), and the amounts varied from cultivar to cultivar. The maximum amount of momilactone A was 495 nmol g^{-1} FW in 'Urasan 1' (WRC51). Momilactone B was detected in 31 cultivars, and its amounts also showed large variation (Figure 2.2b). The amount of momilactone B in each cultivar was generally smaller than that of momilactone A. The cultivars that accumulate large amounts of momilactone A tended to accumulate larger amounts of momilactone B (Figure 2.2c). The japonica cultivars tended to accumulate larger amounts of momilactones than the indica cultivars.

The analysis was also performed in the wild rice species because momilactones and phytocassanes accumulate in several wild rice species in the genus *Oryza* (Miyamoto *et al*., 2016). We analyzed *O. rufipogon* Griff., *O. barthii* A. Chev., *O. glaberrima* Steud., *O. glumaepatula* Steud., and *O. meridionalis* N. Q. Ng with the same AA genome as *O. sativa*, *O. punctata* Kotschy ex Steud. with the BB genome, and *O. brachyantha* A. Chev. Et Rhoer. with the FF genome. The BB genome is most closely related to the AA genome, whereas the FF genome diverged at the basal part of the phylogenetic tree of genus *Oryza* (Stein *et al*., 2018).

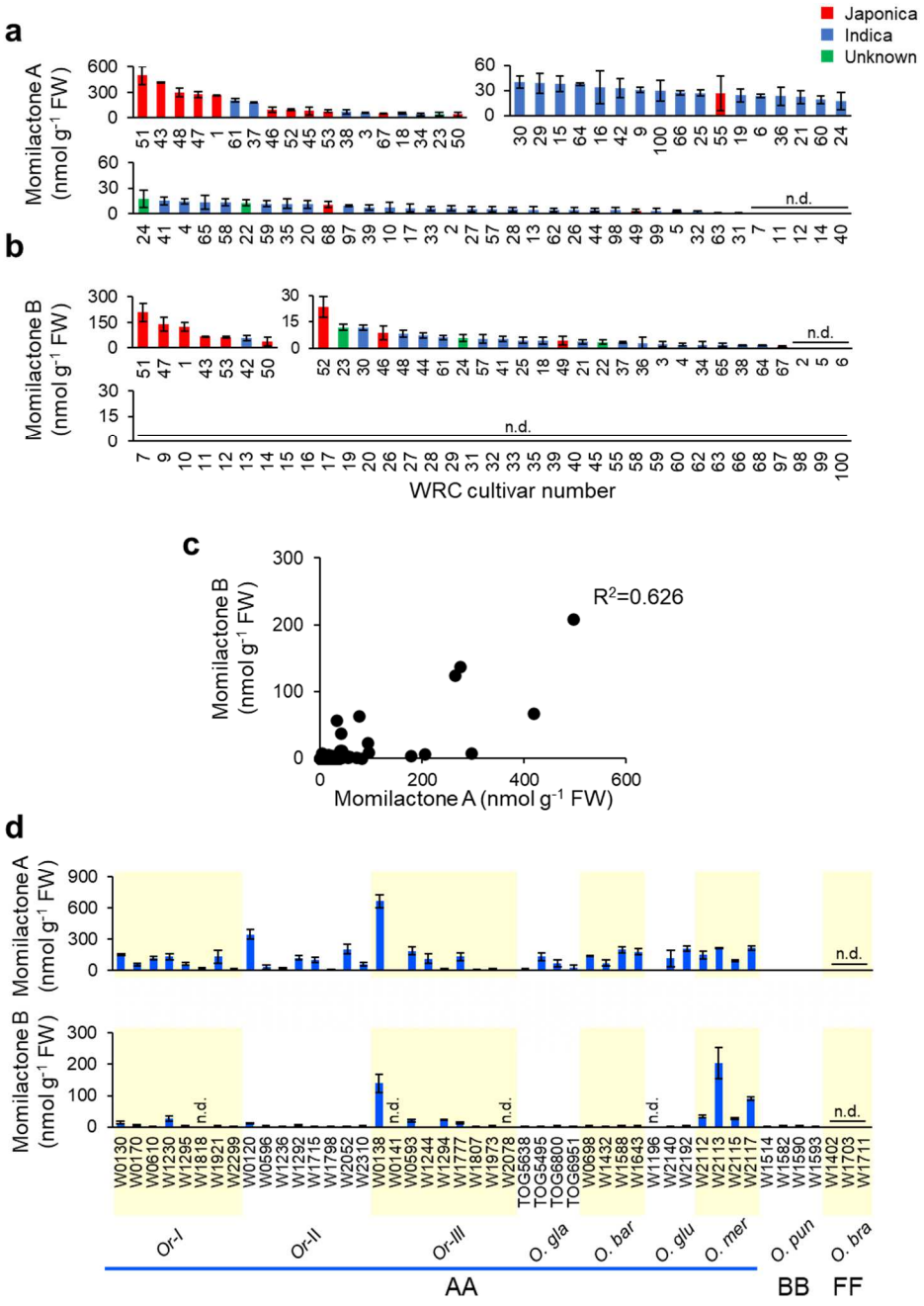

Figure 2.2. Accumulation of momilactones A and B in cultivars from the WRC and wild rice species after UV irradiation. (**a**) Momilactone A amounts in WRC cultivars. (**b**) Momilactone B amounts in WRC cultivars. (**c**) Correlation between the amounts of momilactones A and B. R^2: decision coefficient. (**d**) Amounts of momilactones A and B in wild rice species. *Or*-I, *Or*-II, and *Or*-III indicate clades of *O. rufipogon*. *O. gla*: *O. glaberrima*; *O. bar*: *O. barthii*; *O. glu*: *O. glumaepatula*; *O. mer*: *O. meridionalis*; *O. pun*: *O. punctata*; *O. bra*: *O. brachyantha*. AA: AA genome species; BB: BB genome species; FF: FF genome species. Values are means ± SD of three biological replicates. n.d.: not detected.

Momilactone A was detected in all AA and BB genome species that we analyzed (Figure 2.2d). The amounts in BB genome species (0.97–2.76 nmol g^{-1} FW) were much smaller than those in AA genome species (1.36–667 nmol g^{-1} FW). Momilactone B was also detected in all AA and BB genome species (Figure 2.2d). However, one *Or*-I (W1818) and two *Or*-III (W0141 and W2078) strains, and one *O. glumaepatula* (W1196) strain did not accumulate momilactone B. By contrast, momilactones A and B were not detected in *O. brachyantha*, which is an FF genome species.

Phytocassanes A and D were detected in all cultivars except 'Jinguoyin' (WRC11) (Figures 2.3a and 2.3b). The largest amounts of phytocassanes A and D were 899 and 217 nmol g^{-1} FW, respectively. Phytocassane A was more abundant than phytocassane D in all cultivars. The amounts of phytocassanes A and D varied in parallel among the cultivars. There was a good correlation between the amounts of phytocassanes A and D (Figure 2.3c).

A large variation in the accumulation of phytocassanes A and D was also observed in the wild rice species (Figure 2.3d). Phytocassane A was detected in all AA genome species, except W1196 (*O. glumaepatula*). Phytocassane D was not detected in strains that accumulated little or no phytocassane A, two *Or*-III strains (W1777 and W1973), and one *O. glumaepatula* strain (W1196). *O. punctata*, a BB genome species, did not accumulate either phytocassanes A or D, whereas phytocassane A was detected in *O. brachyantha*, an FF genome species.

During the analysis of the amounts of momilactone A by multiple reaction monitoring (MRM) mode in LC-MS/MS, we noticed the two peaks of unknown compounds **1** and **2** in 'Jaguary' (WRC47) and 'Basilanon' (WRC44), respectively, as shown in Figure 2.4. These peaks were not detected in extracts from leaves that had not

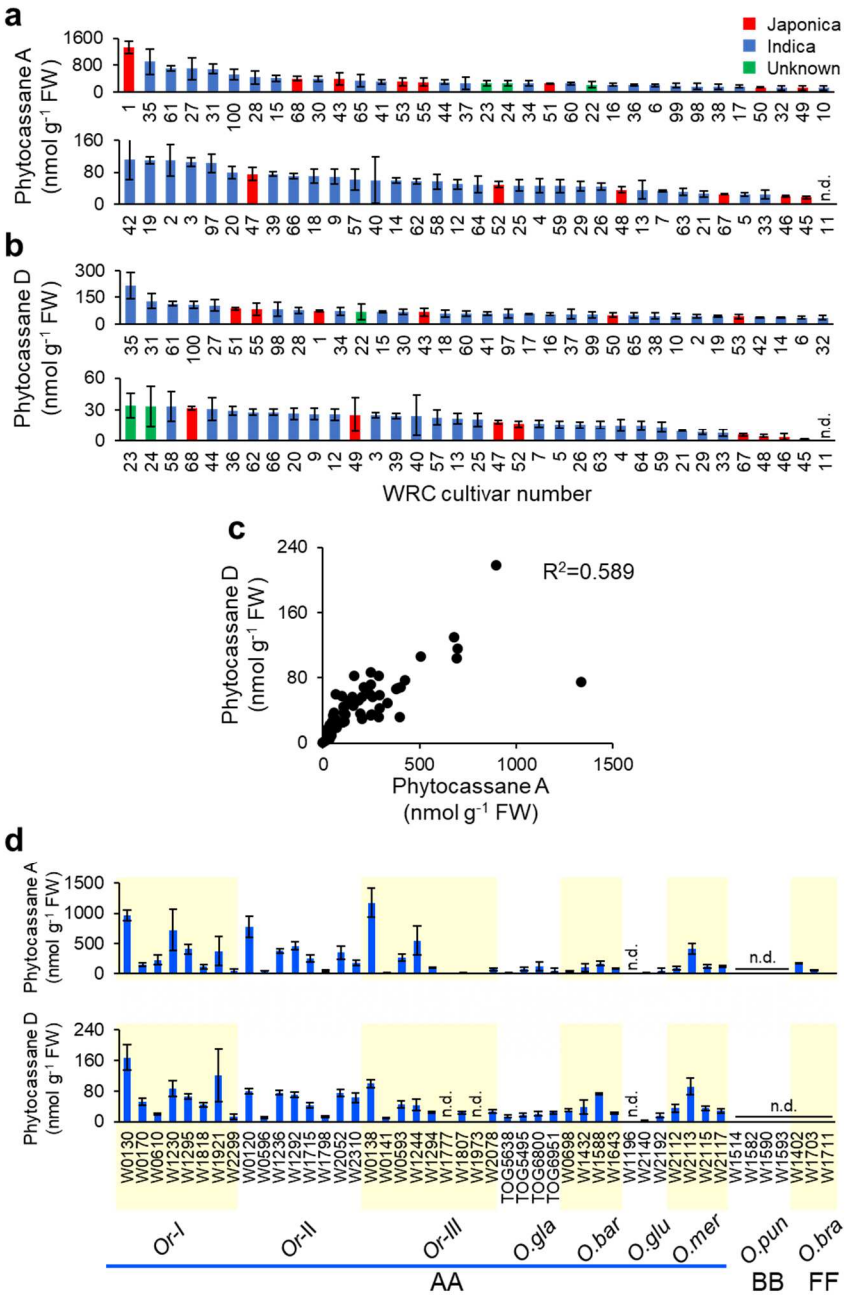

Figure 2.3. Accumulation of phytocassanes A and D in cultivars from the WRC and wild rice species after UV irradiation. (**a**) Phytocassane A amounts in WRC cultivars. (**b**) Phytocassane D amounts in WRC cultivars. (**c**) Correlation between the amounts of phytocassanes A and D. R^2: decision coefficient. (**d**) Amounts of phytocassanes A and D in wild rice species. *Or*-I, *Or*-II, and *Or*-III indicate clades of *O. rufipogon*. *O. gla*: *O. glaberrima*; *O. bar*: *O. barthii*; *O. glu*: *O. glumaepatula*; *O. mer*: *O. meridionalis*; *O. pun*: *O. punctata*; *O. bra*: *O. brachyantha*. AA: AA genome species; BB: BB genome species; FF: FF genome species. Values are means ± SD of three biological replicates. n.d.: not detected.

been UV irradiated.

Identification of 1

Compound **1** was purified by silica gel and ODS column chromatography and preparative HPLC from 'Jaguary' (WRC47) leaves that had been irradiated with UV light. Compound **1** had the molecular formula $C_{20}H_{26}O_3$, as determined by HRMS (*m/z* 315.1952 $[M + H]^+$). The hydrogen deficiency index was determined to be 8.

The ^1H NMR (Table 2.1) and HMQC spectra of **1** suggested the presence of four methyl groups [δ_H 1.02 (overlapped), 1.03, and 1.51 ppm], four methylene groups (δ_H 1.63–2.97 ppm), and four methine groups (δ_H 2.14, 2.21–2.26, 2.32, and 4.81 ppm). All protonated carbon atoms were assigned by HMQC. Two ^1H NMR signals (δ_H 5.41 and 5.80 ppm) and four ^{13}C NMR signals (δ_C 112.3, 117.5, 144.2, and 148.2 ppm, Table 2.1) indicated the presence of two double bonds. The double-bond protons were not coupled with each other. In addition, the presence of two quaternary carbon atoms (δ_C 53.5 and 32.3 ppm) and two carbonyl groups (δ_C 174.4 and 205.3 ppm) were indicated by the ^{13}C NMR spectrum. Because no active proton was detected, the signals at δ_C 174.4 and 73.3 ppm suggested an ester linkage. Considering the molecular formula and above-mentioned

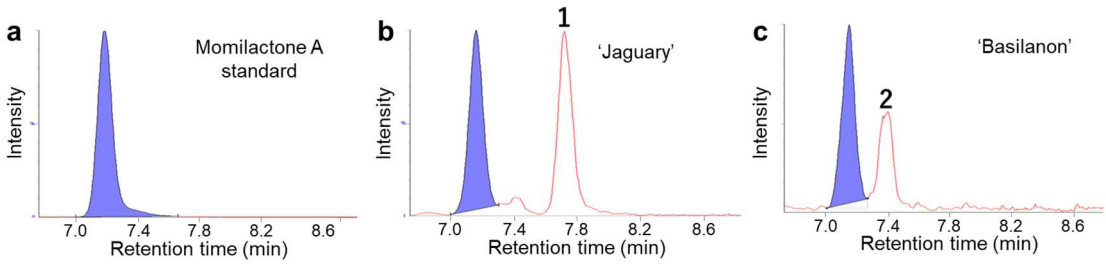

Figure 2.4. Multiple reaction monitoring (MRM) chromatogram in momilactone A analysis. (**a**) Analysis of authentic momilactone A; retention time of 7.2 min. (**b**) Compound **1** was detected in the extract from 'Jaguary' with a retention time of 7.7 min. (**c**) Compound **2** was detected in the extract from 'Basilanon' with a retention time of 7.4 min.

Table 2.1. ^{1}H (600 MHz) and ^{13}C NMR (150 MHz) data of **1** and momilactone A in $CDCl_3$

Position	**1**		Momilactone A[a)]	
	δH ppm; multi; *J* in Hz	δC ppm	δH ppm; multi; *J* in Hz	δC ppm
1	1.89; dq; 3.0, 11.7, 18.6 1.633; m; 3.0, 7.8, 13.2	31.0	1.9; dd 1.5-1.65; complex	34.89
2	2.60-2.64; m; overlapped 2.60-2.64; m; overlapped	34.8 [*1]	2.58-2.69; complex 2.58-2.69; complex	31.25
3		205.3		205
4		53.5		53.57
5	2.32; d; 5.4	46.2 [*2]	2.32; d	46.67
6	4.81; dt; 1.2, 4.8, 6.0	73.3	4.84; t; 5	73.17
7	5.80; d; 4.8	112.3	5.71; d; 5	114.06
8		148.2		147.98
9	2.14; dd; 6.0, 12.0	46.3 [*2]	1.80; dd	50.24
10		32.3		32.52
11	1.96; m 2.21-2.26; m; overlapped	28.5	1.32; complex [*4] 1.75; complex [*4]	24.03
12	5.41; t; 2.7, 2.7	117.5	1.5-1.65; complex	37.25
13		144.2		40.16
14	2.67; d; 17.4 2.97; d; 17.4	37.2	2.21; d 12.5 2.06; d	47.57
15	2.21-2.26; m; overlapped	34.9 [*1]	5.85; dd; 10.5, 13	148.95
16	1.02-1.03	21.2 [*3]	4.95; dd 4.98; dd; 1	110.12
17	1.02-1.03	21.7 [*3]	0.90; s	21.97
18	1.51; s	21.7 [*3]	1.52; s	21.47
19		174.4		174.25
20	1.02; s	21.8 [*3]	1.00; s	21.78

a) Cartwright et al. (1981) Phytochemistry 20: 535-537.

* Assignments of the signals with the same number may be interchanged.

partial structures, Compound **1** is assumed to be an isomer of momilactone A (Figures 2.5a and 2.5b). The ^{1}H and ^{13}C NMR spectra of **1** were similar to those of momilactone

A, but the chemical shifts of the protons and carbon signals at the 12, 13, 15, and 16 positions of **1** were largely different from those of momilactone A (Table 2.1). On the basis of the COSY and HMBC spectra, a double bond (δ_H 5.41 ppm; δ_C 117.5 and 144.2 ppm) was located between the 12 and 13 positions in **1**. The signal of H-15 showed correlations with two methyl groups at the 16 and 17 positions on the COSY spectrum (Figure 2.5a), suggesting the presence of an isopropyl group. The signals of C-15 and C-16 were shifted to higher magnetic field for **1** than those for momilactone A, indicating saturation of the double bond present at these positions in momilactone A. Based on these analyses, we constructed the structure of **1** as shown in Figure 2.5a. The correlations detected in the HMBC spectrum supported the proposed structure without inconsistencies. The relative stereochemistry of **1** was determined from the NOESY spectrum (Figure 2.5c). Cross peaks were detected for H-1/H-9, H-1/H-20, and H-9/H-20. In addition, the

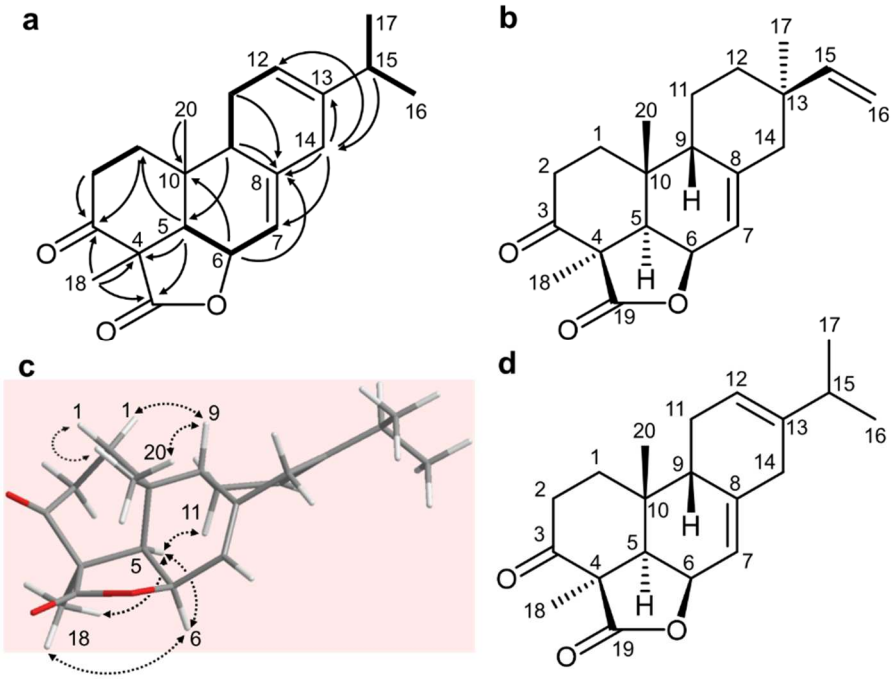

Figure 2.5. Analysis of the chemical structure of **1**. (**a**) COSY (bold lines) and HMBC (black arrows from protons to carbon atoms) correlations of **1**. (**b**) Chemical structure of momilactone A. (**c**) NOESY correlations on the three-dimensional chemical structure of **1**. (**d**) Chemical structure of **1**.

spectrum showed cross peaks for H-5/H-6, H-5/H-11, H-5/H-18, and H-6/H-18. These correlations suggested that **1** had the same relative configuration as momilactone A. According to the CD spectra, **1** and momilactone A showed negative Cotton effects at 299 and 297 nm, respectively. Therefore, the structure of **1** was determined to be 9β-abieta-3-one-7,12-diene-19,6β-olide, and we named this compound as oryzalactone (Figure 2.5d).

Identification of 2

Compound **2** was purified in a similar way to the purification of **1** from 'Basilanon' (WRC44) leaves that had been irradiated with UV light for 72 h. The molecular formula of **2** was determined to be $C_{20}H_{26}O_3$ by HRMS (*m/z* 337.1772 $[M + Na]^+$). The hydrogen deficiency index was 8.

The ^1H NMR spectrum (Table 2.2) indicated the presence of four methyl groups (δ_H 1.11, 1.13, 1.23, and 1.24 ppm) and three double bonds, which correspond to a terminal olefin (δ_H 5.50, 5.68, and 6.36 ppm) and two isolated double bonds (δ_H 5.79 and 5.94 ppm). According to the ^{13}C NMR spectrum, two carbonyl groups were observed (δ_C 200.3 and 200.8 ppm, Table 2.2). Based on the ^1H NMR and HMQC spectra, there were two methylene groups [δ_H 1.55 (overlapped), 1.70 (overlapped), and 1.80 ppm], four methine groups [δ_H 1.70, 2.28 (two protons were overlapped), and 2.65 ppm], two quaternary carbon atoms (δ_C 39.0 and 44.3 ppm), and one hydroxy group (δ_H 5.96 ppm). This hydroxy group was considered to bind to an olefinic carbon atom because no signal for an sp^3 carbon atom bearing an oxygen atom was detected on the ^{13}C NMR spectrum. On the basis of these partial structures, we assumed that **2** is a derivative of phytocassane A. The molecular formula of **2** was consistent with di-dehydrogenated phytocassane A. A comparison of the ^1H and ^{13}C NMR spectra of **2** with those of phytocassane A (Figures

2.6a and 2.6b, Table 2.2) indicated that the chemical shifts of the proton and carbon signals of **2** were similar to those of phytocassane A, except at the 1 and 2 positions. The carbon atoms at the 1 and 2 positions were considered to form a double bond because of

Table 2.2. ^{1}H (600 MHz) and ^{13}C NMR (150 MHz) data of **2** and phytocassane A in $CDCl_3$

Position	**2**		Phytocassane A[a)]	
	δH ppm; multi; *J* in Hz	δC ppm	δH ppm; multi; *J* in Hz	δC ppm
1	7.68; s	129.2	2.32; dd; 7.9, 14.7	50.5
			2.83; br dd; 11.5, 14.7	
2		143.8	4.63; dd; 7.9, 11.5	68.6
3		200.3		219
4		44.3		45.8
5	1.70; m; overlapped	52.7	1.94, dd, 3.3, 12.2	51.6
6	1.55; m; overlapped	21.0	1.45; dddd; 3.3, 12.2,12.5, 13.0	22.4
	1.70; m; overlapped		1.68; dddd, 3.3, 3.3, 3.3, 13.0	
7	1.55; m; overlapped	30.9	1.56; dddd; 3.3, 12.5, 12.5, 12.5	30.4
	1.80; m		1.77, dddd, 3.3, 3.3, 3.3, 12.5	
8	2.28; m; overlapped	38.5	2.06; dddd; 3.3, 4.3, 12.5, 13.0	38.3
9	2.28; m; overlapped	52.5	2.23; d; 13.0	56.4
10		39.0		36.8
11		200.8		200.3
12	5.79; s	128.5	5.78; s	128.4
13		161.1		160.7
14	2.65; dq; 3.0, 7.2	33.6	2.68; dq; 4.3, 7.2	32.9
15	6.36; dd; 10.8, 18.0	136.4	6.36; dd; 10.9,17.7	136.2
16	5.68; d; 18.0	121.0	5.69; br d; 17.7	120.9
	5.50; d; 10.8		5.51; br d; 10.9	
17	1.11; d; 7.2	13.4	1.12; d; 7.2	13.5
18	1.23; s	26.9	1.14; s	19.4
19	1.13; s	22.3	1.17; s	29.6
20	1.24; s	18.2	0.80; s	16.8
2OH	5.96; s		3.51; br s	

[a)] Koga *et al.* (1995) Tetrahedron **51**: 7907-7918.

their chemical shifts (δ_C 129.2 and 143.8 ppm). Furthermore, the signal of the active proton (δ_H 5.96 ppm) showed cross peaks with C-1 and C-3 (δ_C 129.2 and 200.3 ppm) in the HMBC spectrum (Figure 2.6a). Thus, this hydroxy group was connected to C-2. Accordingly, **2** was suggested as 1,2-di-dehydrogenated phytocassane A.

The relative stereochemistry of **2** was determined from the NOESY spectrum (Figure 2.6c). NOESY correlations indicated that H-6, H-7α, H-8, H-14, H-18, and H-20 were located on the same side of the condensed ring system and H-5, H-7β, H-17, and H-19 were on the other side. Thus, **2** had the same relative configuration as phytocassane A. The absolute stereochemistry of **2** was determined by a comparison of the CD spectrum of **2** with that of phytocassane A. The spectrum of **2** was similar to that of phytocassane A. Therefore, **2** was determined to be 2-hydroxy-*ent*-1,12,15-cassatriene-3,11-dione (Figure 2.6d), and we named **2** as phytocassane G.

We initially detected phytocassane G by the MRM method developed for momilactone A, with the monitored mass transition from *m/z* 315 to *m/z* 271. We could

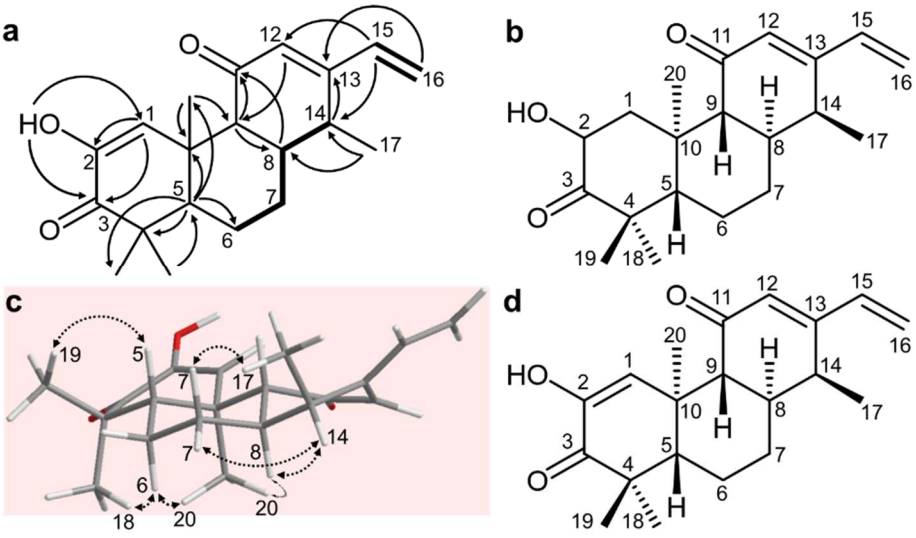

Figure 2.6. Analysis of the chemical structure of **2**. (**a**) COSY (bold lines) and HMBC (black arrows from protons to carbon atoms) correlations of **2**. (**b**) Chemical structure of phytocassane A. (**c**) NOESY correlations on the three-dimensional chemical structure of **2**. (**d**) Chemical structure of **2**.

not determine the chemical structure of the fragment ion at *m/z* 271 generated from phytocassane G. The sensitivity of this MRM method toward phytocassane G was 840-fold lower than that toward momilactone A, indicating that the ion at *m/z* 271 generated from phytocassane G was the product of a minor fragmentation reaction. In cultivars that accumulated high concentrations of Momilactone A, the peaks of momilactone A and phytocassan G were not sufficiently separated, and the phytocassan G peak merged with the momilactone A peak. Therefore, we modified the analytical method for diterpenoid phytoalexins by LC-MS/MS in the MRM mode before quantitative analysis. The analytical conditions are summarized in Table S2.3 together with the detection limits of the compounds.

We analyzed the amounts of oryzalactone and phytocassane G in 'Jaguary' and 'Basilanon' leaves, respectively, inoculated with conidia of rice blast fungus. The amount of oryzalactone was 66 nmol g^{-1} FW 72 h after inoculation, which is around 14 times greater than that in the control leaves (Figure 2.7a). Accumulation of phytocassane G was also induced by pathogen attack; the amount detected was 119 nmol g^{-1} FW (Figure 2.7b), whereas phytocassane G was not detected in the control leaves.

Antifungal activities of oryzalactone and phytocassane G

The antifungal activities of oryzalactone and phytocassane G, together with those of momilactone A and phytocassane A, were examined by inhibition assays for the conidia germination and germ tube elongation of *Pyricularia oryzae* Cavara 1892 [syn: *Magnaporthe oryzae* (Catt.) BC Couch 2002, Magnaporthaceae]. Germination of conidia was inhibited by 86% and 45% in the presence of a 300 μM concentration of oryzalactone and phytocassane G, respectively, and no conidia germination was detected at 1,000 μM

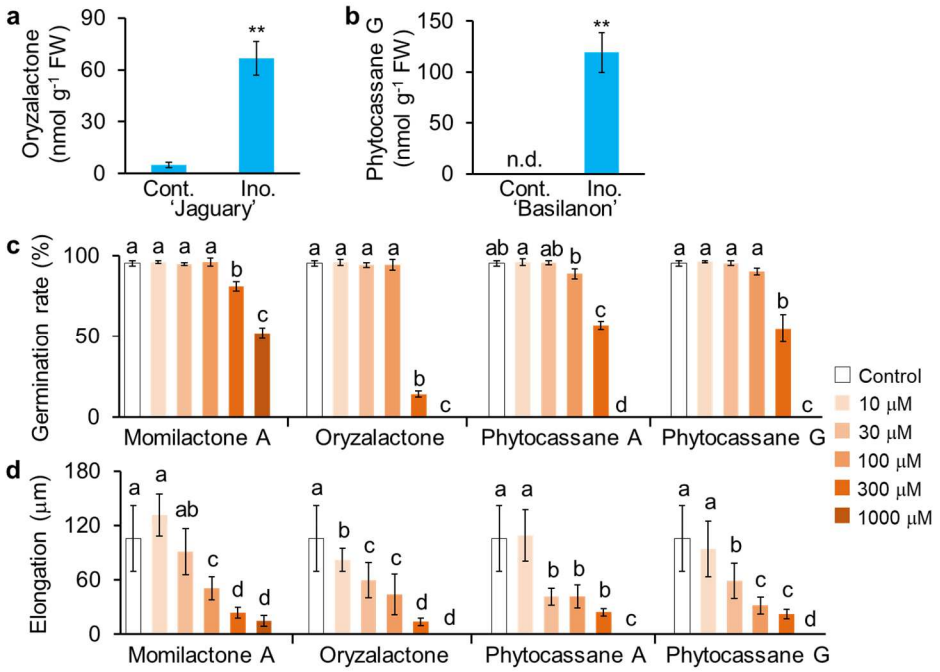

Figure 2.7. Accumulation of oryzalactone and phytocassane G in response to rice blast infection and the antifungal activities of these compounds against rice blast. (**a**) Accumulation of oryzalactone in 'Jaguary' leaves in response to rice blast infection. (**b**) Accumulation of phytocassane G in 'Basilanon' leaves in response to rice blast infection. Amounts of **1** and **2** were determined 72 h after the start of treatment. n.d.: not detected. Values are means ± SD of three biological replicates. Asterisks indicate significant differences (*p < 0.05, **p < 0.01; Dunnett's test). (**c**) Effect of compounds on the germination of *P. oryzae* 12 h after incubation. (**d**) Effect of compounds on conidial germ tube elongation, which was measured 12 h after treatment. Values and error bars are means ± SD (n = 3). Different letters indicate significant differences ($p < 0.05$; Tukey–Kramer method).

for either compound (Figure 2.7c). The inhibitory activity of oryzalactone on conidia germination was slightly higher than that of momilactone A. The activity of phytocassane G was almost the same as that of phytocassane A. The germ tube elongation of conidia of *P. oryzae* was significantly inhibited by oryzalactone and phytocassane G at concentrations higher than 30 μM (Figure 2.7d). The inhibitory activities of momilactone A and oryzalactone, and phytocassanes A and G were almost the same.

Accumulation of oryzalactone and phytocassane G in various rice cultivars and wild rice species

Oryzalactone and phytocassane G were purified from the leaves of 'Jaguary' and 'Basilanon', respectively, but momilactones and phytocassanes accumulated in almost all cultivars in the WRC. We investigated the generality of the accumulation of oryzalactone and phytocassane G by using cultivars from the WRC. Oryzalactone was detected in only three cultivars, WRC42, WRC47, and WRC68 (Figure 2.8a). The amounts (16.5–48.1 nmol g^{-1} FW) were smaller than those of momilactone A in the same cultivars. By contrast, almost all cultivars accumulated phytocassane G, and only two cultivars (WRC11 and WRC67) lacked this compound (Figure 2.8b). The amount of phytocassane G in the cultivars reached a maximum of 55.2 nmol g^{-1} FW ('ARC5955', WRC35) and was not greater than the amount of phytocassanes A or D in most cultivars. The accumulation of oryzalactone was limited to a small number of wild rice strains, which were three *Or*-II (W0120, W1236, and W2052), one *Or*-III (W1777), and one *O. meridionalis* (W2117) strains, with the accumulated amount being 2.5–38.6 nmol g^{-1} FW (Figure 2.8c). Phytocassane G was detected in all of the analyzed AA genome species, with the amount being 2.0–137.2 nmol g^{-1} FW, but it was not detected in *O. punctata* and *O. brachyantha* (Figure 2.8c).

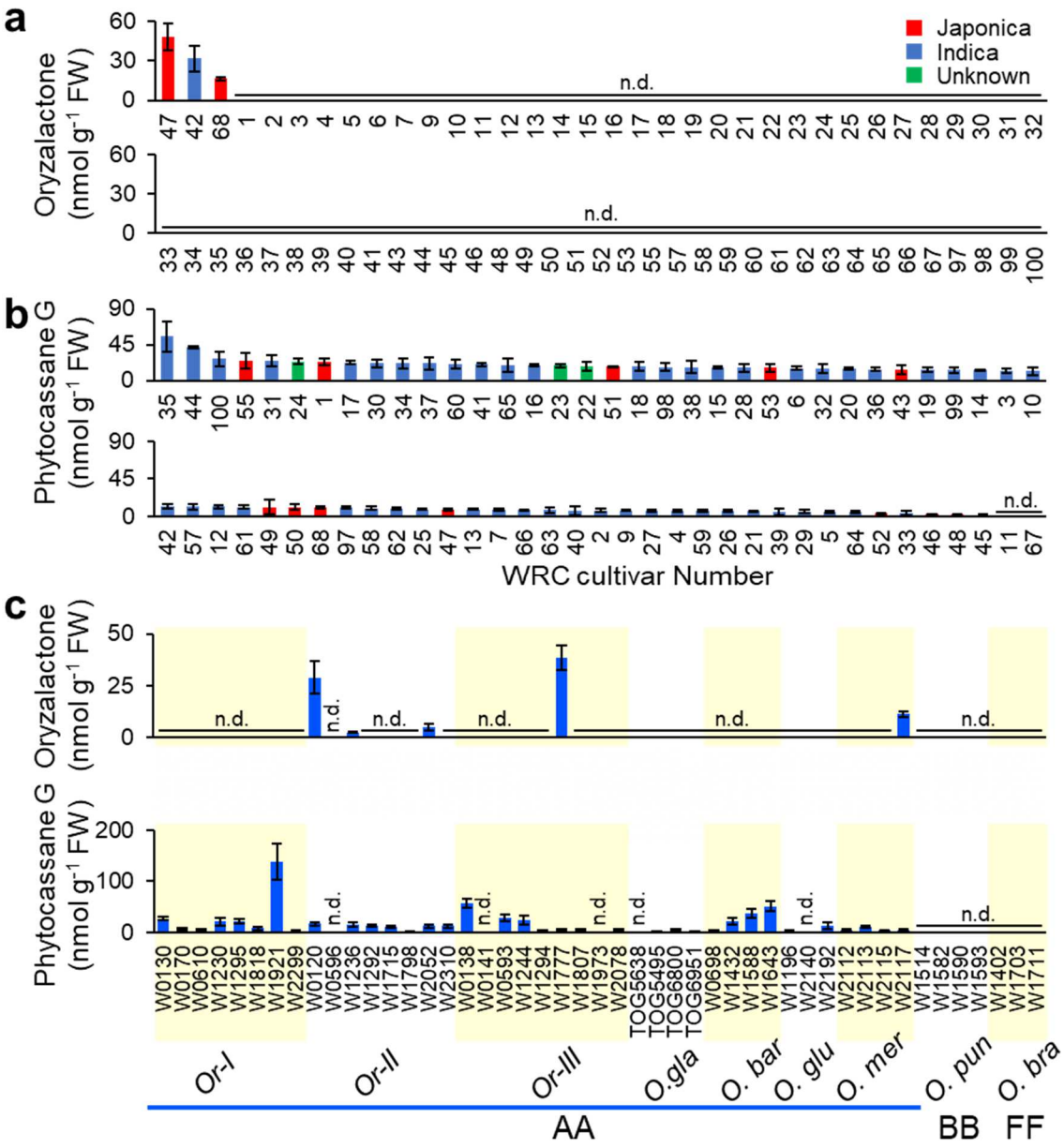

Figure 2.8. Accumulation of oryzalactone and phytocassane G in the WRC cultivars and wild rice species after UV irradiation. (**a**) Oryzalactone amounts in WRC cultivars. (**b**) Phytocassane G amounts in WRC cultivars. (**c**) Oryzalactone and phytocassane G amounts in wild rice species. *Or*-I, *Or*-II, and *Or*-III indicate clades of *O. rufipogon*. *O. gla*: *O. glabberima*; *O. bar*: *O. barthii*; *O. glu*: *O. glumaepatula*; *O. mer*: *O. meridionalis*; *O. pun*: *O. punctata*; *O. bra*: *O. brachyantha*. AA: AA genome species; BB: BB genome species; FF: FF genome species. Values are means ± SD of three biological replicates. n.d.: not detected.

2-3 Discussion

We analyzed the accumulation of diterpenoid phytoalexins in multiple *O. sativa* cultivars. Two chemotypes, oryzalexin A-accumulating and oryzalexin A-lacking, were observed in rice. The accumulated amounts of momilactones A and B varied among cultivars from the WRC, and some japonica cultivars accumulated these compounds at high concentrations. A large variation in the accumulated amounts of phytocassanes was also found in the WRC cultivars. Similar large variations were also observed in wild rice species. Thus, it is reasonable to assume that the different chemotypes in the accumulation of phytoalexins originate, at least partly, from *O. rufipogon* during the evolution of rice.

Since **1** had a lactone ring and a different carbon skeleton from known phytoalexins of rice, we named **1** as oryzalactone. On the other hand, **2** was named as phytocassane G because it had a common carbon skeleton with other phytocassanes. The accumulation of these compounds was induced by infection with rice blast fungus, as well as by UV irradiation. Moreover, oryzalactone and phytocassane G inhibited conidia germination and germ tube elongation, which indicates that they have antifungal activity against *P. oryzae*. The activities were in a similar range to those of momilactone A and phytocassane A. Based on these findings, oryzalactone and phytocassane G are well-suited for definition as phytoalexins.

Oryzalactone is a diterpenoid with abietane skeleton. In this respect, oryzalactone is different from other reported rice diterpenoid phytoalexins. Six kaurene synthase homologs (kaurene synthase like: KSL) have been isolated and characterized in rice, but no KSLs have been shown to function as abietadiene synthases (Kanno *et al*., 2006; Xu *et al*., 2007). It is known that a single substitution of an amino acid residue in a kaurene synthase causes the generation of different products. OsKSL5 in japonica and

indica rice subspecies produces *ent*-pimara-8(14),15-diene and *ent*-isokaurene, respectively. This difference was attributable to a single amino acid substitution from Ile^{664} to Thr^{664} (Xu *et al*., 2007). A mutation in a KSL in the specific lineage might have caused the generation of oryzalactone.

Phytocassane G is regarded as a compound that has an additional double bond generated by dehydrogenation at the 1 and 2 positions in phytocassane A. In many cases, the double bond of cyclic diterpenes is introduced after the generation of a carbocation during the cyclization step catalyzed by kaurene synthase like enzymes. However, in this case, because the C-1 and C-2 atoms are distant from the carbocation generated during the cyclization step, the double bond is likely introduced by modification of the cyclization product. The biosynthetic pathway of phytocassanes has been greatly elucidated; yet many of the biosynthetic genes remain unknown (Ye *et al*., 2018). Many pathways leading to the generation of phytocasane G can be hypothesized; that is, phytocassanes A, B, D, or F could be the precursor of phytocassane G (Supplementary Figure S2.1). Oxidation at the 2 and 3 positions of phytocassanes A and D would result in the formation of *ent*-12,15-cassadiene-2,3,11-trione, which could be converted into phytocassane G by keto–enol tautomerism. Alternatively, dehydration at the 1 and 2 positions of phytocassane F or dehydration at the 1 and 2 positions with oxidation at the 3 position of phytocassane B would generate phytocassane G.

Miyamoto *et al*. (2016) suggested that *O. punctata* and *O. brachyantha* lost the biosynthetic genes for phytocassanes because phytocassanes C and E accumulated in *Leersia perrieri*, which is a species outside of the genus *Oryza*. We detected phytocassane A in all AA genome species and the FF genome species *O. brachyantha*, but not in the BB genome species *O. punctata*. The difference between our result on the accumulation

of phytocassane A in *O. brachyantha* and that of Miyamoto *et al*. (2016) is attributable to the natural variation in this species; indeed, W1711 in *O. brachyantha* did not accumulate phytocassane A. Notably, *O. brachyantha* did not accumulate either phytocassane D or G, despite the fact that this species accumulates phytocassane A. This result implies a close biosynthetic relationship between phytocassanes D and G. The biosynthetic pathways to phytocassane D and G might have been acquired in the lineage to AA genome species, or the pathway for these phytocassanes might have been lost in the lineage to FF genome species after splitting of the FF genome lineage from the AA genome lineage.

2-4 Experimental

General experimental procedure

^{1}H and ^{13}C NMR spectra and ^{1}H-^{1}H COSY, HMQC, HMBC, and NOESY spectra were recorded by using an Avance II instrument (Bruker, Billerica, MA, USA). High-resolution mass spectra were measured by using an Exactive mass spectrometer (Thermo Fisher Scientific, Waltham, MA, USA). LC-MS/MS analysis and ESI-MS measurement were performed by using a Quattro Micro API mass spectrometer (Waters, Milford, MA, USA) that was connected to an Acquity UPLC system (Waters). HPLC analyses were performed with a 10A HPLC system (Shimadzu, Kyoto, Japan). CD spectra were measured by using a J-820 circular dichroism spectrometer (JASCO, Tokyo, Japan).

Plant materials and pathogenic fungi

The WRC (Kojima *et al*., 2005), *Oryza sativa* L., and African rice, *Oryza glaberrima* Steud., were provided by the National Agriculture and Food Research Organization (NARO) genebank (https://www.gene.affrc.go.jp/index_j.php). Seeds of wild rice species (*Oryza rufipogon* Griff., *Oryza barthii* A. Chev., *Oryza glumaepatula* Steud., *Oryza meridionalis* N. Q. Ng, *Oryza punctata* Kotschy ex Steud., and *Oryza brachyantha* A. Chev. Et Rhoer.) were obtained from the National Institute of Genetics (NIG; https://www.nig.ac.jp/nig/ja/). Among the *O. meridionalis* strains, W2113, W2115 and W2117 are described as *O. rufipogon*/*O. meridionalis* on the database (Rice Database Oryzabase: https://shigen.nig.ac.jp/rice/oryzabase/) and we regarded these three strains as *O. meridionalis* strains. Rice strains used in this study were listed in Tables S2.1 and S2.2.

Rice blast fungus (*Pyricularia oryzae* Cavara 1892; syn. *Magnaporthe oryzae*

(Catt.) B.C. Couch 2002, race 007, Naga 69–150) came from the stock culture of the Laboratory of Plant Pathology, Shimane University.

Induction of phytoalexin production

Rice seeds were sown on a 1:4 mixture of vermiculite (Shoei Sangyo, Okayama, Japan) and artificial compost for rice (Grin Grow, Okayama, Japan) and then incubated at 28°C with a 16 h/8 h light/dark cycle until the third leaves developed. The third leaves were excised from the seedlings, placed on moist paper, and irradiated with UV light (GL-15 germicidal lamp, Hitachi, Tokyo, Japan) for 10 min. The leaves were incubated for 72 h at 28°C in an airtight bag to maintain high humidity.

P. oryzae was cultured on oatmeal-medium agar plates for 20 days. Aerial hyphae were washed away with a brush after adding distilled water, and the plates were incubated for a further 3 days under a black light lamp (FL15BLB, Hitachi, Tokyo, Japan). Synchronously formed conidia were used for inoculation. The conidia were suspended in distilled water containing 0.25% Tween-20, washed twice by centrifugation at 1000×*g* for 3 min, and resuspended in distilled water containing 0.25% Tween-20. Droplets (5 μL) of the conidial suspension (5×10^5 conidia mL^{-1}) were then placed at five points on the third leaves of 18-day-old seedlings at 1-cm intervals. The inoculated seedlings were kept in a moist chamber for 24 h, taken out of the chamber, and incubated for 48 h at 28°C with a 16 h/8 h light/dark cycle.

Analysis of phytoalexins

Authentic compounds, momilactones A and B, phytocassanes A and D, and oryzalexin A, were purified from rice leaves. The rice leaves were irradiated with UV light for 10 min.

The leaves were incubated for 72 h, and the metabolites in the leaves were extracted with 20 vol. of 80% methanol for 48 h. The extract was concentrated and partitioned with ethyl acetate. The ethyl acetate extract was fractionated by silica gel and ODS column chromatography. Finally, compounds were purified by preparative HPLC with an ODS column (Cosmosil AR-II, 20 × 250 mm, Nacalai Tesque, Kyoto, Japan). The identity of the compound was confirmed by ^{1}H NMR spectrum (Cartwright *et al*., 1981; Akatsuka *et al*., 1983; Koga *et al*., 1995).

Rice leaves induced to produce phytoalexin production were cut into 1-cm segments and immersed in 20 vol. of 80% methanol for 48 h. The extract was subjected to LC-MS/MS analysis in MRM mode. The LC conditions were as follows: column: Acquity UPLC BEH C18 column (2.1 × 50 mm, 1.7 μm) (Waters); flow rate: 0.2 mL min^{-1}; column temperature: 40°C; solvents: 0.1% aqueous formic acid (A) and 0.1% formic acid in acetonitrile (B); gradient: 42% (2 min) and then 42–47% B/(A + B) (8 min). Compounds were analyzed in positive ion mode with nitrogen as the collision gas. The monitored precursor-to-product transitions are described in Table S2.3. A methanol solution of authentic compounds at 20 μg mL^{-1} was used as an external standard. The detection limits for phytoalexins with our analytical system is summarized in Table S2.3.

Isolation of unidentified compounds

9β-Abieta-3-one-7,12-diene-19,6β-olide (oryzalactone; compound **1**) was purified from 350 g of ‘Jaguary’ leaves irradiated with UV light. The leaves of rice seedlings were irradiated with UV light for 10 min. The leaves were incubated for 72 h, and the metabolites in the leaves were extracted with 20 vol. of 80% methanol for 48 h. The

extract was concentrated and partitioned with ethyl acetate. The ethyl acetate extract was concentrated, and the resulting residue was subjected to silica gel (Daiso, Osaka, Japan) column chromatography. Compounds were eluted with mixtures of ethyl acetate–*n*-hexane (20:80, 30:70, 40:60, 50:50, v/v). The ethyl acetate–*n*-hexane (30:70 and 40:60) fractions were combined and concentrated by evaporation, and the residue was applied to an ODS column that was preequilibrated with methanol–water (50:50, v/v). The column was eluted with mixtures of methanol–water (50:50, 60:40, 70:30, 80:20, 100:0, v/v). Because oryzalactone was eluted in the 60% methanol fraction, this fraction was concentrated and subjected to repeated preparative HPLC. The first HPLC conditions were as follows: column: Cosmosil 5C18-AR-II column (20 × 250 mm; Nacalai Tesque, Kyoto, Japan); solvents: 65% B/(A+B), A: water, B: acetonitrile; flow rate: 7.0 mL min^{-1}; column temperature: 40°C; detection: 210 nm. Oryzalactone was eluted at 22.5 min. For the second HPLC purification, the solvent was changed to 75% B/(A+B), A: water, B: methanol. The peak corresponding to oryzalactone was detected at 22.0 min, collected, and concentrated to dryness to yield 3.3 mg as white powder.

Oryzalactone: CD spectra (Δε): −0.46 (299 nm), 0.00 (256 nm), −8.55 (217 nm) (10 μg mL^{-1}, ethanol); UV spectra (10 μg mL^{-1}, ethanol): λ_{max} nm (ε): 203 (9120). ^{1}H and ^{13}C NMR data are summarized in Table 2.1.

The CD and UV spectra of momilactone A were measured for comparison. CD spectra (Δε): −1.23 (297 nm), −0.04 (250 nm), −21 (206 nm) (10 μg mL^{-1}, ethanol); UV spectra (10 μg mL^{-1}, ethanol): λ_{max} nm (ε): 203 (11,500).

2-Hydroxy-*ent*-1,12,15-cassatriene-3,11-dione (phytocassane G; compound **2**) was purified from 295 g 'Basilanon' leaves irradiated with UV light. The extracts were subjected to silica gel and ODS column chromatography in a similar way to the purification of oryzalactone. The fraction containing phytocassane G was then subjected to repeated preparative HPLC. The first HPLC conditions were as follows: column: Cosmosil 5C18-AR-II column (20 × 250 mm); solvents: 68% B/(A+B), A: water, B: acetonitrile; flow rate: 7.0 mL min^{-1}; column temperature: 40°C; detection: 210 and 280 nm. Phytocassane G was eluted at 21.5 min. For the second HPLC purification, the solvent and column temperature were changed. Solvent: 65% B/(A+B), A: water, B: methanol; column temperature: 30°C. Phytocassane G was eluted at 60.0 min. The peak corresponding to phytocassane G was collected and concentrated to dryness to yield 3.7 mg as yellow gum.

Phytocassane G: CD spectra (Δε): −0.97 (368 nm), 0.92 (323 nm), −3.04 (284 nm), 2.06 (258 nm), −3.07 (222 nm) (10 μg mL^{-1}, ethanol); UV spectra (10 μg mL^{-1}, ethanol): λ_{max} nm (ε): 271 (16,300). The ^{1}H and ^{13}C NMR data are summarized in Table 2.2.

The spectra of phytocassane A were measured for comparison. CD spectra (Δε): −0.98 (368 nm), 0.07 (320 nm), −2.48 (288 nm), 2.45 (260 nm), −3.69 (222 nm) (10 μg mL^{-1}, ethanol); UV spectra (10 μg mL^{-1}, ethanol): λ_{max} nm (ε): 267 (9,590).

Antimicrobial activity

Droplets of a conidial suspension (100 μL, 5.0×10^4 conidia mL^{-1}) in solutions of momilactone A, oryzalactone, phytocassanes A and G containing 1% DMSO were placed

on a glass slide and incubated at 25°C in the dark. The number of germinated conidia was counted 12 h after the start of incubation under a microscope (BX43; Olympus, Tokyo, Japan). The germ tube lengths were measured with Image J (https://imagej.nih.gov/ij/docs/install/windows.html) software.

Chapter 3
Identification of aromatic diterpenoid phytoalexins in specific cultivars

3-1 Introduction

We quantitatively analyzed five diterpenoid phytoalexins accumulation in various rice cultivars in chapter 2. The amount of each phytoalexin accumulated in the leaves varied widely between the cultivars, demonstrating the intraspecific diversity of phytoalexin accumulation in rice.

Some cultivars accumulated very low levels of diterpenoid phytoalexins. In particular, a cultivar from China ‘Jinguoyin’ (WRC11) did not accumulate any analyzed diterpenoid phytoalexins at detectable levels although phytoalexins have been reported to be important for disease resistance (Toyomasu *et al*., 2014; Lu *et al*., 2018; Zhang *et al*., 2021; Li *et al*., 2022). Therefore, ‘Jinguoyin’ might have developed physical defenses, such as the accumulation of phenolic polymers in the cell walls, rather than chemical defense mechanisms including the accumulation of antimicrobial compounds. Alternatively, the concentration of phytoanticipins, constitutively accumulating antimicrobial compounds, in ‘Jinguyoin’ may be higher than other cultivars. In addition, it is plausible that ‘Jinguoyin’ accumulate non-diterpenoid compounds such as flavonoids and phenylamides as phytoalexins.

Thus, we focused on the accumulation of phytoalexins that specifically accumulate in ‘Jinguoyin’ with the aim of identifying variation in chemical defense in rice cultivars.

3-2 Results

Analysis of inducible metabolites in 'Jinguoyin'

In a previous study, we found that leaves of 'Jinguoyin' did not accumulate known diterpenoid phytoalexins after UV treatment. Thus, 'Jinguoyin' may accumulate different phytoalexins from other cultivars. To investigate the diversity of chemical defense mechanisms within rice species, we analyzed the presence of inducible metabolites in the leaves of the 'Jinguoyin' cultivar. The metabolites were extracted from leaves infected with *Bipolaris oryza*e (Breda de Haan) Shoemaker and were analyzed by LC-MS. To find compounds specifically accumulating in the leaves of 'Jinguoyin', the metabolites in 'Nipponbare' (*japonica* subspecies) and 'Kasalath' (*indica* subspecies), which accumulate known diterpenoid phytoalexins, were also analyzed. The data obtained by LC-MS analysis were subjected to metabolic profiling using a metabolomics program (MarkerLynx, Waters). Six hundred forty and six hundred thirty peaks were detected in positive and negative ion modes, respectively. From these ions, we selected ions having the highest intensities in the pathogen-inoculated leaves of 'Jinguoyin', and 113 positive ions and 78 negative ions were selected. Then, clustering analysis of the selected ions was performed (Figures S3.1a and S3.1b), and six positive ions were selected as ions specifically detected in the pathogen-inoculated leaves of 'Jinguoyin'. The six selected ions were detected only in the inoculated leaves but not in intact and mock inoculated leaves (Figure S3.1c), indicating that they are derived from inducible compounds. The compounds corresponding to these six ions were designated **3**–**7** based on the order of their retention times in the LC-MS analysis (Figure S3.1c).

Structural analyses of 3–7

Compounds **3**–**7** (Figure 3.1) were purified from UV-light-irradiated leaves of 'Jinguoyin' because their accumulation was effectively induced by UV-light irradiation (Figure S3.2). The UV-light-irradiated leaves were incubated for 72 h, and then, extraction with 80% methanol was carried out. The induced compounds were purified using column chromatography and preparative HPLC.

Compound **3** had the molecular formula $C_{20}H_{28}O_3$, as determined by high-resolution (HR)-MS (*m/z* 339.1934 $[M + Na]^+$ and *m/z* 355.1673 $[M + K]^+$). The hydrogen deficiency index is 7.

The ^1H NMR signals in the aromatic region (δ_H 7.14, 7.16, and 7.24 ppm, Table 3.1) indicated the presence of a 1,3,4-trisubstituted benzene ring. Furthermore, the ^1H NMR and HMQC spectra of **3** showed the presence of four methyl groups (δ_H 1.04, 1.15, 1.23, and 1.23 ppm), four methylene groups (δ_H 1.89–4.01 ppm), and three methine groups (δ_H 2.19, 2.87, and 4.83 ppm). The presence of two active protons was inferred

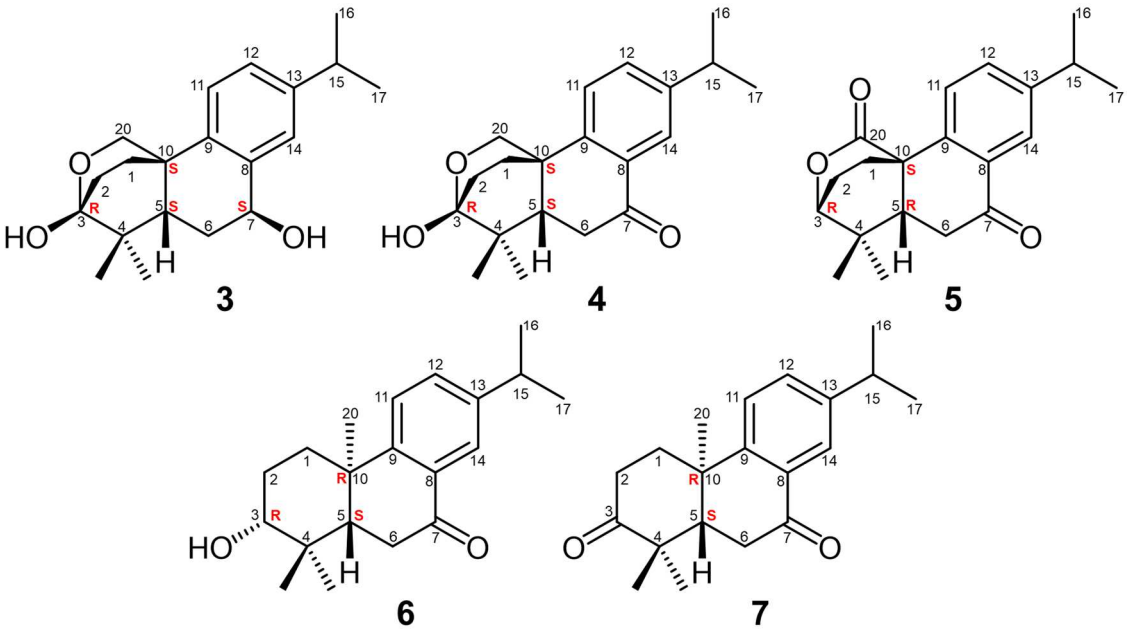

Figure 3.1. Structures of abietoryzins A–E (**3**–**7**).

Table 3.1. ^{1}H NMR (600 MHz) spectroscopic data of abietoryzins A–C in $CDCl_3$.

Position	Abietoryzin A (**3**)	Abietoryzin B (**4**)	Abietoryzin C (**5**)
	ppm (multi; *J* in Hz)	ppm (multi; *J* in Hz)	ppm (multi; *J* in Hz)
1α	2.47 (ddd; 12.0, 12.0, 5.4)	2.57 (ddd; 12.6, 12.6, 5.4)	2.51 (ddd; 13.2, 11.4, 4.2)
1β	1.69 (dddd; 12.6, 12.0, 3.6, 3.0)	1.70 (dddd; 13.8, 10.8, 3.6, 3.6)	1.89 (ddd; 13.2, 10.8, 6.0)
2α	1.92 (ddd; 13.2, 12.0, 3.6)	1.99 (ddd; 13.2, 12.0, 4.2)	2.23 (m; overlapped)
2β	2.31 (ddd; 12.0, 12.0, 6.0)	2.30 (ddd; 13.2, 12.0, 4.8)	2.23 (m; overlapped)
3	–	–	4.32 (dd; 4.2, 1.8)
5	2.19 (m)	2.20 (ddd; 15.6, 4.2, 1.8)	2.34 (dd; 15.0, 3.6)
6α	1.88 (ddd; 13.8, 13.8, 3.0)	2.74 (dd; 15.6, 15.6)	2.45 (dd; 15.0, 15.0)
6β	2.02 (ddd; 13.8, 3.0, 3.0)	2.66 (dd; 15.6, 4.2)	2.70 (dd; 15.0, 3.6)
7	4.83 (m)	–	–
11	7.24 (d; 8.4)	7.31 (d; 8.4)	7.35 (d; 7.8)
12	7.16 (dd; 8.4, 2.4)	7.41 (dd; 8.4, 2.4)	7.50 (dd; 7.8, 1.8)
14	7.14 (d; 2.4)	7.85 (d; 2.4)	7.90 (d; 1.8)
15	2.87 (sept; 6.6)	2.92 (sept; 7.2)	2.96 (sept; 7.2)
16	1.23 (d; 6.6)	1.237* (d; 7.2)	1.26 (d; 7.2)
17	1.23 (d; 6.6)	1.238* (d; 7.2)	1.26 (d; 7.2)
18	1.04 (s)	1.07 (s)	1.13 (s)
19	1.15 (s)	1.13 (s)	1.20 (s)
20α	4.01 (dd; 9.6, 3.0)	4.25 (dd; 9.0, 3.6)	–
20β	3.93 (dd; 9.6, 1.8)	4.05 (dd; 9.0, 1.8)	–

* Assignments may be interchanged.

from the molecular formula and ^{1}H NMR data. All protonated carbon atoms were assigned based on the HMQC data. In addition, three quaternary carbons (δ_C 35.7, 40.0, and 99.2 ppm) were detected in the ^{13}C NMR spectra (Table 3.2). Based on the molecular formula and chemical shifts of the signals in the ^{1}H NMR spectrum, this molecule contains three oxygen atoms and three carbon atoms (δ_C 68.4, 71.8, and 99.2 ppm) bearing oxygen atoms. The carbon atom corresponding to the signal at δ_C 99.2 ppm was

Table 3.2. ^{13}C NMR (150 MHz) spectroscopic data of abietoryzins A–C in $CDCl_3$.

Position	Abietoryzin A (**3**)	Abietoryzin B (**4**)	Abietoryzin C (**5**)
	ppm	ppm	ppm
1	34.4	34.0	31.3
2	29.5	29.4	22.0
3	99.2	98.9	84.9
4	40.0	40.4	37.9
5	40.5	46.5	48.1
6	28.2	36.7	38.8
7	68.4	198.7	197.3
8	136.2	132.1	132.0
9	137.6	141.9	138.5
10	35.7	36.2	46.2
11	127.0*	126.8	128.8
12	127.1*	132.6	132.8
13	147.8	148.1	148.8
14	128.1	124.8	124.7
15	33.7	33.7	33.8
16	24.0	23.8	23.7*
17	23.9	23.8	23.8*
18	18.2	18.2	22.4
19	26.7	27.0	27.8
20	71.8	70.8	175.0

*Assignments may be interchanged.

considered to be bonded to two oxygen atoms because of its low field shift. Therefore, the presence of ester bond was suggested. Correlation between the signal at δ_H 2.87 ppm and two methyl groups (δ_H 1.23 and 1.23 ppm) in the ^1H-^1H COSY spectrum suggested that these signals correspond to an isopropyl group.

These substructures were connected based on the correlations detected in the ^1H-^1H COSY and heteronuclear multiple-bond correlation (HMBC) spectroscopy spectra to construct the structure of **3** shown in Figure 3.2.

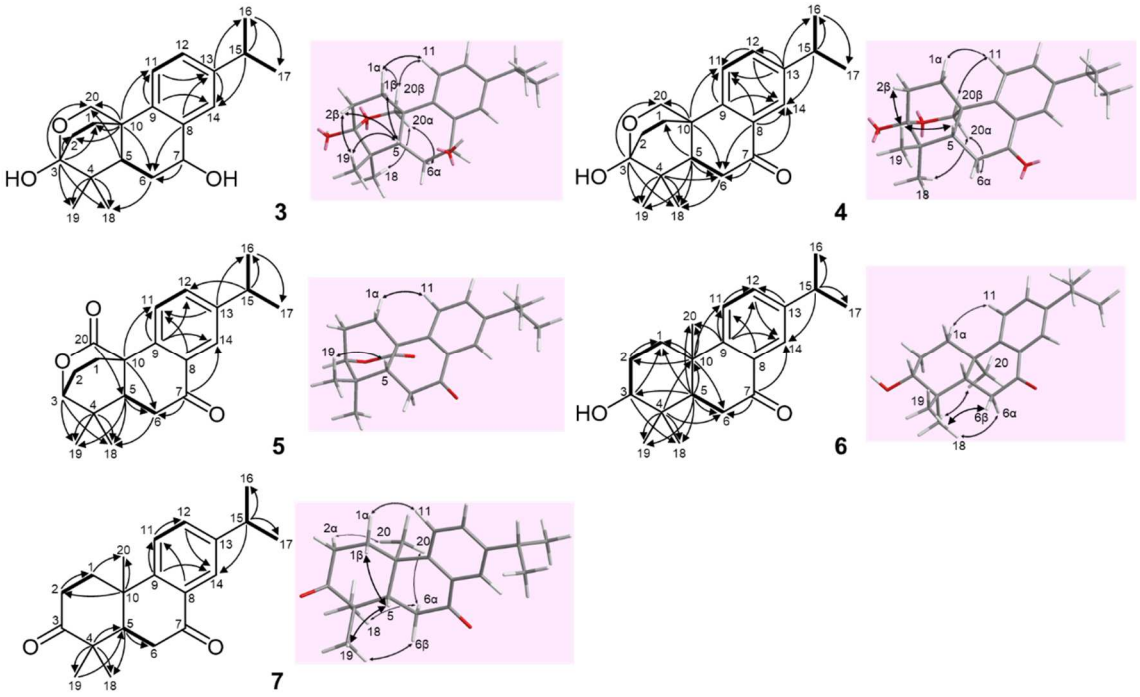

Figure 3.2. Structural analysis of **3**–**7**. ^{1}H-^{1}H COSY and HMBC correlations are shown by bold lines and black arrows from carbon atoms to protons, respectively, and NOESY correlations are shown as arrows on the three-dimensional chemical structure.

The relative stereochemistry of **3** was determined based on its NOESY spectrum (Figure 3.2). NOESY correlations indicated that H-1β (δ_H 1.69 ppm), H-2β (δ_H 2.31 ppm), H-5 (δ_H 2.19 ppm), and H-19 (δ_H 1.15 ppm) were located on the same side of the condensed ring system, and H-6α (δ_H 1.88 ppm), H-18 (δ_H 1.04 ppm), and H-20α (δ_H 4.01 ppm) were on the other side. Finally, the absolute structure of **3** was determined by the crystalline sponge method (Figures S3.3 and S3.4), and thus, **3** was determined to be 3α,20α-epoxy-3β,7β-dihydroxy-5β-abieta-8,11,13-triene.

Compound **4** had the molecular formula $C_{20}H_{26}O_3$, as determined by HR-MS (*m/z* 315.1960 $[M + H]^+$, *m/z* 337.1780 $[M + Na]^+$, and *m/z* 313.1804 $[M - H]^-$). The hydrogen deficiency index is 8.

The ^{1}H NMR signals in the aromatic region (δ_H 7.31, 7.41, and 7.85 ppm, Table

3.1) indicated a 1,3,4-trisubstituted benzene ring. The ^{1}H NMR and HMQC spectra of **4** showed the presence of four methyl (δ_H 1.07, 1.13, 1.237, and 1.238 ppm), four methylene (δ_H 1.70–4.25 ppm), and two methine (δ_H 2.20 and 2.92 ppm) groups. All protonated carbon atoms were assigned using HMQC. In addition, three quaternary carbons (δ_C 36.2, 40.4, and 98.9 ppm) and a carbonyl carbon (δ_C 198.7 ppm) were observed in the ^{13}C NMR (Table 3.2) and HMQC spectra.

In addition to the oxygen and carbon atoms of the carbonyl group, this molecule contains two oxygen atoms and two carbon atoms (δ_C 70.8 and 98.9 ppm) bearing oxygen atoms. The signal at δ_C 98.9 ppm was considered to be derived from a quaternary carbon bonded to two oxygen atoms because of its chemical shift. The presence of a hydroxyl group was suggested by the molecular formula and ^{1}H NMR spectrum. Thus, it was deduced that carbons at δ_C 98.9 and 70.8 ppm are connected via an oxygen atom and that the signal at δ_C 98.9 ppm corresponds to a hemiacetal carbon. The signal at δ_H 2.92 ppm showed correlations with signals of two methyl groups (δ_H 1.237 and 1.238 ppm) in ^{1}H-^{1}H COSY spectrum, indicating that the signals correspond to an isopropyl group. These substructures were connected based on ^{1}H-^{1}H COSY and HMBC spectra to obtain the structure of **4** shown in Figure 3.2. The correlation detected in the NOESY spectrum was used to predict the relative stereochemistry, as shown in Figure 3.2. The absolute stereochemistry of **4** was determined by single crystal X-ray diffraction analysis (Figure S3.5); thus, **4** was identified as 3α,20α-epoxy-3β-hydroxy-5β-abieta-8,11,13-triene-7-one.

Li *et al*. (2014) reported the enantiomer of **4** from rice husks. The authors did not describe the reason for the assignment of the absolute stereochemistry, but, because the direction of specific rotation was the same as that of **4**, the previously isolated compound

was considered to have the same absolute stereochemistry as **4**.

Compound **5** had a molecular formula of $C_{20}H_{24}O_3$, as determined by HR-MS (*m/z* 313.1803 $[M + H]^+$, 335.1697 $[M + Na]^+$, and 311.1697 $[M - H]^-$). The hydrogen deficiency index was 9.

The ^1H NMR signals in the aromatic region (δ_H 7.35, 7.50, and 7.90 ppm, Table 3.1) indicated a 1,3,4-trisubstituted benzene ring. The ^1H NMR and HMQC spectra of **5** showed the presence of four methyl (δ_H 1.13, 1.20, and 1.26 ppm), three methylene (δ_H 1.89–2.70 ppm), and three methine (δ_H 2.34, 2.96, and 4.32 ppm) groups. All protonated carbon atoms were assigned based on the HMQC data. In addition, two quaternary (δ_C 37.9 and 46.2 ppm) and two carbonyl (δ_C 175.0 and 197.3 ppm) carbons were detected in the ^{13}C NMR spectrum (Table 3.2). Because no active proton was predicted in the structure, the signals at δ_C 175.0 and 84.9 ppm suggest the presence of an ester linkage. The signal at δ_H 2.96 ppm showed correlations with two methyl groups (δ_H 1.26 and 1.26 ppm) in ^1H-^1H COSY spectrum, suggesting the presence of an isopropyl group. These substructures were connected based on the ^1H-^1H COSY and HMBC spectra to construct the structure of **5** shown in Figure 3.2. The correlation detected in the NOESY spectrum was used to predict the relative stereochemistry, as shown in Figure 3.2. The absolute stereochemistry of **5** was finally determined using the crystalline sponge method (Figures S3.6 and S3.7), and thus, **5** was identified as 5β-abieta-8,11,13-triene-7-one-3α,20α-olide.

Compound **6** has the molecular formula of $C_{20}H_{28}O_2$, as determined by HR-MS (*m/z* 323.1987 $[M + Na]^+$ and 339.1726 $[M + K]^+$). The hydrogen deficiency index was determined as 7.

The ^1H NMR signals in the aromatic region (δ_H 7.26, 7.40, and 7.87 ppm, Supplementary Table S3.1) indicate the presence of a 1,3,4-trisubstituted benzene ring.

The ^{1}H NMR and HMQC spectra of **6** showed the presence of five methyl (δ_H 0.97, 1.05, 1.240, 1.242, and 1.246 ppm), three methylene (δ_H 1.70–2.73 ppm), and three methine (δ_H 1.79–1.91, 2.92, and 3.35 ppm) groups. On the basis of the ^{1}H NMR spectrum and molecular formula, an active proton was expected. All protonated carbon atoms were assigned based on the correlations in the HMQC spectrum. In addition, two quaternary carbons (δ_C 37.7 and 39.0 ppm) and a carbonyl carbon (δ_C 199.6 ppm) were detected in the ^{13}C NMR spectrum (Supplementary Table S3.2). The correlations between the signal at δ_H 2.92 ppm and signals corresponding to two methyl groups (δ_H 1.242 and 1.246 ppm) in the ^{1}H-^{1}H COSY spectrum indicate an isopropyl group. These substructures were connected based on the ^{1}H-^{1}H COSY and HMBC spectra to construct the structure of **6** shown in Figure 3.2. The correlations detected in the NOESY spectrum suggest the relative stereochemistry shown in Figure 3.2, and the absolute stereochemistry of **6** was determined using the crystalline sponge method (Figures S3.8 and S3.9), and thus, **6** was identified as 3α-hydroxy-5β,20α-abieta-8,11,13-trien-7-one. Compound **6** was already reported from *Ceriops decandra* and the NMR data was consistent with those reported by Jiang *et al*. (2018).

Compound **7** has the molecular formula $C_{20}H_{26}O_2$, as determined by HR-MS (*m/z* 299.2009 $[M + H]^+$, 321.1809 $[M + Na]^+$, and 297.1853 $[M - H]^-$). The hydrogen deficiency index was 8.

The ^{1}H NMR signals in the aromatic region (δ_H 7.28, 7.43, and 7.90 ppm, Supplementary Table S3.1) indicated the presence of a 1,3,4-trisubstituted benzene ring. The ^{1}H NMR and HMQC spectra of **7** showed the presence of five methyl (δ_H 1.14, 1.20, 1.250, 1.253, and 1.44 ppm), three methylene (δ_H 2.02–2.89 ppm), and two methine (δ_H 2.33 and 2.94 ppm) groups. All protonated carbon atoms were assigned based on the

HMQC spectra. In addition, two quaternary (δ_C 37.0 and 47.5 ppm) and two carbonyl (δ_C 198.5 and 214.6 ppm) carbons were detected in the ^{13}C NMR spectrum (Supplementary Table S3.2). The signal at δ_H 2.94 ppm was correlated with two methyl signals (δ_H 1.250 and 1.253 ppm) in the ^{1}H-^{1}H COSY spectrum, indicating the presence of an isopropyl group. These substructures were connected based on the ^{1}H-^{1}H COSY and HMBC spectra to construct the structure of **7** shown in Figure 3.2. The correlations detected in the NOESY spectrum were used to predict the relative stereochemistry shown in Figure 3.2, and the absolute stereochemistry of **7** was determined using the crystalline sponge method (Figures S3.10 and S3.11), and thus, **7** was identified as 5β,20α-abieta-8,11,13-triene-3,7-dione. Compound **7** was already reported from *Ceriops decandra*, and the NMR data was consistent with those reported by Jiang *et al*. (2018).

Compounds **3** and **5** have not been described previously, and compounds **4**, **6**, and **7** do not have a trivial name. Therefore, compounds **3**–**7** were named abietoryzins A–E, respectively.

Antimicrobial activities of abietoryzins A–E

The antifungal activities of abietoryzins A–E were examined using inhibition assays for the conidial germination and germ tube elongation of *Pyricularia oryzae*, the causal agent of rice blast, and *B. oryzae*, the causal agent of rice brown spot (Table 3.3, Figure S3.12). All abietoryzins inhibited the germ tube elongation of both phytopathogenic fungi, and their effective concentrations were lower than the those found in the conidial germination assay; the IC_{50} values for germ tube elongation were more than 10 times smaller than those for conidial germination. It is of interest to note that abietoryzins A, D, and E showed relatively strong activity among abietoryzins for *P. oryzae* germ tube elongation

Table 3.3. IC_{50} values of abietoryzins A–E for the inhibition of conidial germination and germ tube elongation of *Pyricularia oryzae* and *Biopolaris oryzae* and for the growth inhibition of *Xanthomonas oryzae* and *Burkholderia glumae*.

	Germ Tube Elongation		Conidial Germination		Bacterial Growth	
Abietoryzins	*P. oryzae*	*B. oryzae*	*P. oryzae*	*B. oryzae*	*X. oryzae*	*B. glumae*
	μM	*μM*	*μM*	*μM*	*μM*	*μM*
A (**3**)	6.6	10.3	844	>1000 (27)[a]	>1000 (0)	>1000 (0)
B (**4**)	20.1	9.8	>1000 (6)	>1000 (22)	>1000 (0)	>1000 (15)
C (**5**)	21.9	9.8	587	>1000 (23)	>1000 (8)	>1000 (25)
D (**6**)	7.8	31.5	182	519	>1000 (28)	>1000 (19)
E (**7**)	8.1	21.2	>1000 (44)	>1000 (16)	>1000 (0)	>1000 (0)

[a]The values in parentheses are inhibition rates (%) at 1000 μM.

but abietoryzins B and C showed strong activity for *B. oryzae*.

The antibacterial activity of abietoryzins was examined by the growth inhibition of *Burkholderia glumae* Kurita and Tabei, and *Xanthomonas oryzae* pv. *oryzae* (Ishiyama) Dye, the causal agents of rice bacterial grain rot and bacterial leaf blight, respectively. All compounds did not inhibit the growth of these bacterial pathogens by more than 50% (Table 3.3). Abietoryzins B–D showed growth inhibitory activity against *B. glumae* at 1,000 μM, whereas abietoryzins A and E did not (Figure S3.12e). The growth of *X. oryzae* was not significantly affected by these compounds at tested concentrations (Figure S3.12f).

Accumulation of abietoryzins A–E in various rice cultivars

Abietoryzins A–E were purified from the leaves of 'Jinguoyin', which, as mentioned, almost completely lacks the accumulation of known diterpenoid phytoalexins. The WRC is a core collection of 69 varieties, some of which accumulate only low levels of

diterpenoid phytoalexins. Thus, we examined the possibility that other cultivars in the WRC also accumulated abietoryzins (Figures 3.3 and S3.13).

Abietoryzin A was accumulated in 12 cultivars in the WRC, and 'Jinguoyin' accumulated abietoryzin A at the highest concentration (1,060 nmol g^{-1} fresh weight (FW)) among the WRC cultivars (Figure S3.13a). Abietoryzins B–E accumulated in 22–30 out of 69 WRC cultivars. The maximum amounts of abietoryzins B–E were 797, 382, 321, and 264 nmol g^{-1} FW, respectively (Figures S3.13b–e). Eighteen cultivars among 52 *indica* cultivars accumulated at least one of abietoryzins, whereas six cultivars of the 14 *japonica* cultivars did. The amounts of these accumulated compounds tended to be larger in *indica* cultivars than in *japonica* cultivars. The cultivars accumulating abietoryzin A also tended to accumulate abietoryzins B–E (Figure 3.3a). The amounts of abietoryzins were compared between UV-light irradiated and unirradiated leaves of highly abietoryzins accumulating cultivars (Figure S3.14). The amounts of abietoryzins were undetectable or marginal in UV-light unirradiated leaves.

In addition, we compared the amounts of accumulated momilactones, phytocassanes, oryzalexin A, oryzalactone, and abietoryzins in the WRC cultivars (Figure 3.3). Cultivars accumulating abietoryzins at high concentrations accumulated relatively low levels of known diterpenoid phytoalexins. On the other hand, cultivars accumulating phytocassanes and momilactones at high concentrations accumulated abietoryzins at low concentrations. Subsequently, principal component analysis (PCA) was performed based on the amounts of accumulated diterpenoid phytoalexins in the cultivars from the WRC (Figures 3.3b and 3.3c). The compounds were classified into three groups: abietoryzins, phytocassanes, and momilactones and oryzalexin A (Figure 3.3b). Similarly, PCA was performed to classify the cultivars based on phytoalexin composition (Figure 3.3c). The

analysis did not explicitly classify the cultivars into groups, but the cultivars were widely dispersed. The first principal component reflected phytocassane accumulation, and the positive direction of the second principal component indicated the accumulation of abietoryzins, whereas the negative direction indicated the accumulation of momilactones.

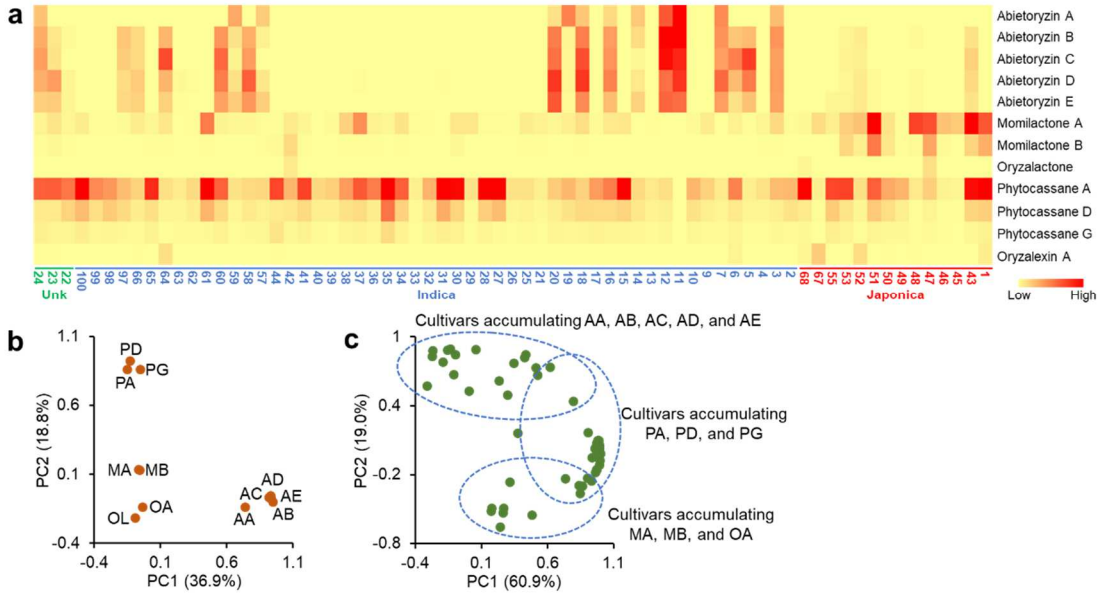

Figure 3.3. Phytoalexin accumulation in samples from the WRC. The accumulated amounts of phytoalexins in the cultivars from the WRC are expressed as a heat map (**a**). PCA analysis was performed based on the amounts of accumulated diterpenoid phytoalexins in the WRC cultivars, and the results are plotted for compounds (**b**) and cultivars (**c**). AA: abietoryzin A, AB: abietoryzin B, AC: abietoryzin C, AD: abietoyzin D, AE: abietoryzin E, PA: phytocassane A, PD: phytocassane D, PG: phytocassane G, MA: momilactone A, MB: momilactone B, OA: oryzalexin A, OL: oryzalactone.

3-3 Discussion

Abietoryzins A–E are diterpenoids that contain a benzene ring. The isolation of abietoryzins A and C from natural sources has not been reported to date. Abietoryzin B has been isolated from rice husks (Li *et al*., 2014) and abietoryzins D and E have been isolated from Godavari mangrove, *Ceriops decandra* (Jiang *et al*., 2018). However, in this study and for the first time, we detected them from pathogen-infected rice leaves. All compounds showed significant inhibitory activities for both the conidial germination and germ tube elongation of *P. oryzae* and *B. oryzae*. Therefore, we conclude that abietoryzins A–E are phytoalexins in rice based on the finding that these compounds are induced by pathogenic infection and possess antimicrobial activities.

The leaves of 'Jinguoyin' accumulated higher concentrations of abietoryzins A–E than the leaves of other cultivars, and the amounts accumulated were sufficient to inhibit the germ tube elongation of fungal pathogens. The antimicrobial activities of abietoryzins A–E are similar to those of momilactone A and phytocassane A (Figure 2.7). Therefore, abietoryzins are considered the dominant phytoalexins in 'Jinguoyin'.

The inhibitory activity on conidial germination differed between compounds: abietoryzin D markedly inhibited conidial germination at 300 μM for both phytopathogenic fungi, whereas abietoryzin B showed no inhibition, even at 1000 μM. However, the inhibitory activity on germ tube elongation was not very different among the abietoryzins, and all compounds significantly suppressed germ tube elongation in both fungi, even at 10 μM. Therefore, the mechanisms of the inhibition of spore germination and germ tube elongation may differ. In addition, abietoryzins showed almost no growth-inhibition activity against bacterial pathogens. Because cultivars accumulating abietoryzins tended to accumulate other diterpenoid phytoalexins at low concentrations

(Figure 3.3a), it is likely that other classes of phytoalexins, such as flavonoids and phenylamides, serve to defend against bacteria.

In the present study, we focused on the inducible metabolites specific to 'Jinguoyin'. However, in the mass spectra, ions specific only to 'Kasalath' or 'Nipponbare' were detected. Furthermore, some ions were detected in both 'Nipponbare' and 'Jinguoyin' but not in 'Kasalath'. These specific ions suggest the presence of additional cultivar-specific phytoalexins and indicate that the intraspecific diversity in inducible metabolites is quite large, as shown for constitutive metabolites in rice (Deng *et al*., 2020; Zhang *et al*., 2022). Abietoryzins are diterpenoids with a benzene ring, and their chemical structures are similar. Based on this, we predicted their biosynthetic pathways, as shown in Figure S3.15. In the shown pathway, geranylgeranyl pyrophosphate (GGPP) is converted into *ent*-copalyl diphosphate (CDP) by CPS2. Subsequently, *ent*-miltiradiene is expected to be produced from *ent*-CDP via an enzymatic reaction, followed by spontaneous aromatization to *ent*-abietatriene (Gao *et al*., 2009; Zi and Peters, 2013). Similar reactions have been proposed for the biosynthesis of triptolide and tanshinones (Forman *et al*., 2017; Wang and Peters, 2022). Toyomasu *et al*. (2016) reported that the homolog of *KSL10*, class I diterpene synthase, in wild rice (*O. rufipogon*) catalyzes the cyclisation of *ent*-CDP to *ent*-miltiradiene. This enzyme might be involved in the biosynthesis of abietoryzins.

The carbons at positions 3 and 7 of abietoryzins are oxidized during biosynthesis, and this oxidization pattern is similar to that of phytocassanes and oryzalexins, suggesting the involvement of common biosynthetic enzymes. Furthermore, abietoryzins A and B resemble momilactone B in the modification at positions 3 and 20, respectively. In the biosynthesis of momilactone B, CYP76M14 has been shown to be responsible for the

oxidation at 20 position (Pena and Sattely, 2021) although it has not been clarified whether the subsequent formation of a hemiacetal occurs via an enzymatic or spontaneous reaction. Thus, the 20-position of 7-hydroxy-abietatriene-3-one (P3 in Figure S3.15) may be oxidized to 7,20-dihydroxy-abietatriene-3-one (P4) by CYP76M14, although the stereochemistry of the methyl group (C-20) differs between abietoryzins and momilactone B (Cartwright *et al*., 1981).

3-4 Experimental

General experimental procedures

Analytical instruments are same with chapter 2.

Plant materials and pathogens

Details of plant materials are described in chapter 2. The *Pyricularia oryzae* strain used is the same with that described in chapter 2. *Bipolaris oryzae* (Breda de Haan) Shoemaker (syn. *Cochliobolus miyabeanus* (Ito & Kurib.) Drechs. ex Dastur) (MAFF 305067), *Xanthomonas oryzae* pv. *oryzae* (Ishiyama) Dye (MAFF 210548), and *Burkholderia glumae* Kurita and Tabei (MAFF 106541) were obtained from NIAS Genebank (http://www.gene.affrc.go.jp/index_en.php).

Induction of phytoalexin production

Plant growth condition and phytoalexin induction by UV-light are described in chapter 2. The inoculation of *B. oryzae* was performed according to a previously described method (Murata *et al*., 2020).

Analysis of induced compounds in B. oryzae*-infected leaves*

The third leaves of 'Jinguoyin', 'Nipponbare', and 'Kasalath' seedlings were inoculated with *B. oryzae.* After a 72-h incubation, the leaves were cut into 1-cm segments and immersed in 20 vol. of 80% methanol for 48 h at 4°C in the dark. The extract was then subjected to LC-MS analysis. The LC and MS conditions were as follows: LC; column: ACQUITY UPLC BEH C18 Column 2.1 × 50 mm (1.7 μm) (Waters); flow rate: 0.2 mL min^{-1}; column temperature: 40°C; solvents: 0.1% aqueous formic acid (A) and

0.1% formic acid in acetonitrile (B); gradient: 5%–100% B/(A+B) (15 min); MS; capillary voltage: 3.00 kV; source temperature: 120°C; desolvation temperature: 350°C; desolvation gas flow: 600 L h^{-1}; cone gas flow: 50 L h^{-1}; range of detection: *m/z* 100–800 (positive and negative); cone voltage: 20 V. The obtained data were subjected to peak-picking analysis using MarkerLynx XS. The analyses were performed separately for the positive and negative ions. The analytical parameters were as follows: positive ions, low *m/z*: 100; high *m/z*: 800; mass tolerance (Da): 1.00; peak width at 5% height: 1,400; peak-to-peak baseline noise: 300,000; intensity threshold: 900,000; mass window: 1.00; retention time window: 0.2; noise elimination level: 5. Negative ions, low *m/z*: 100; high *m/z*: 800; mass tolerance (Da): 1.00; peak width at 5% height: 100,000; peak-to-peak baseline noise: 2,500; intensity threshold: 25,000; mass window: 1.00; retention time window: 0.2; noise elimination level: 5. All the detected peaks were aligned with the retention time and *m/z*. The peak areas for samples were standardized for each ion using z-score normalization, and the scores were averaged. The ions showing the highest z-score in the inoculated 'Jinguoyin' sample were selected to obtain ions unique to this sample. A heatmap was created using the extracted ions, and hierarchical clustering was performed using Pearson's correlation coefficients.

Isolation of induced compounds

The leaves of 'Jinguoyin' seedlings were irradiated with UV light for 10 min. The leaves (285 g) were incubated for 72 h, and the metabolites in the leaves were extracted using 20 vol. of 80% methanol for 48 h at 4°C in the dark. The extract was concentrated and partitioned using ethyl acetate. The ethyl acetate layer was concentrated, and the resulting residue was subjected to silica-gel column chromatography (Daiso, Osaka, Japan). The

compounds were eluted using mixtures of ethyl acetate and *n*-hexane (0: 100, 20: 80, 40: 60, 60: 40, 80: 20, and 100: 0, v/v). Compound **3** was eluted in the 60% ethyl acetate fraction, whereas compounds **4**–**7** were eluted in the 40% ethyl acetate fraction. The 60% ethyl acetate fraction was concentrated and applied to an ODS column pre-equilibrated with water. The column was eluted with mixtures of methanol–water (0: 100, 10: 90, 20: 80, 30: 70, 40: 60, 50: 50, 60: 40, 70: 30, 80: 20, and 100: 0, v/v). Compound **3** was eluted in the 60% methanol fraction. Finally, **3** was purified by preparative HPLC. The 40% ethyl acetate fraction was concentrated and applied to the ODS column. The compounds were eluted with mixtures of methanol and water (40: 60, 50: 50, 60: 40, 70: 30, 80: 20, 90: 10, and 100: 0, v/v). Compounds **4**–**7** were eluted in the 40–60% methanol fractions. The fractions were concentrated and subjected to repeated preparative HPLC. The conditions for the prep. HPLC were as follows: column: Cosmosil 5C18-AR-II (20 × 250 mm; Nacalai Tesque, Kyoto, Japan); flow rate: 7.0 mL min^{-1}; column temp: 40°C; detection: 210 and 280 nm. Different solvent systems were employed for the purification of **3**–**7**: water (A) and acetonitrile (B); composition: 55% B/(A + B) for **3** (*Rt*: 13.0 min) at first prep. HPLC; water (A) and methanol (B); composition: 50% B/(A + B) for **3** (*Rt*: 86.0 min) at second step; water (A) and acetonitrile (B); composition: 63% B/(A + B) for **4**–**7** (*Rt*: 15.0, 18.5, 22.5, and 28.5 min) at first step; water (A) and methanol (B); composition: 70% B/(A + B) for **4** (*Rt*: 22.5 min) and **5** (*Rt*: 20.0 min) at second step; water (A) and methanol (B); composition: 80% B/(A + B) for **6** (*Rt*: 18.4 min) and **7** (*Rt*: 18.5 min) at second step. The peaks corresponding to **3**–**7** were collected and concentrated to dryness to obtain yields of 2.4, 11.2, 2.6, 3.2, and 3.4 mg, respectively.

Abietoryzin A (**3**): CD spectra (Δε): 0.32 (217 nm) (50 μg mL^{-1}, ethanol); UV spectra (50

μg mL^{-1}, ethanol): λ_{max} nm (ε): 216 (5467) and 275 (1213). The ^{1}H and ^{13}C NMR data are summarized in Tables 3.1 and 3.2, respectively.

Abietoryzin B (**4**): CD spectra (Δε): 0.21 (298 nm), −0.56 (243 nm), −0.34 (220 nm) (50 μg mL^{-1}, ethanol); UV spectra (50 μg mL^{-1}, ethanol): λ_{max} nm (ε): 217 (7636), 250 (6990), and 297 (1752). The ^{1}H and ^{13}C NMR data are summarized in Tables 3.1 and 3.2, respectively.

Abietoryzin C (**5**): CD spectra (Δε): 0.52 (298 nm), −0.05 (244 nm), 0.63 (220 nm) (50 μg mL^{-1}, ethanol); UV spectra (50 μg mL^{-1}, ethanol): λ_{max} nm (ε): 218 (6639), 250 (7457), and 295 (1735). The ^{1}H and ^{13}C NMR data are summarized in Tables 3.1 and 3.2, respectively.

Abietoryzin D (**6**): CD and UV spectra data are summarized in Supplementary Information. The ^{1}H and ^{13}C NMR data are summarized in Supplementary Tables S3.1 and S3.2, respectively.

Abietoryzin E (**7**): CD and UV spectra data are summarized in Supplementary Information. The ^{1}H and ^{13}C NMR data are summarized in Supplementary Tables S3.1 and S3.2, respectively.

Single crystal X-ray diffraction analysis and crystalline sponge method

Single crystal X-ray diffraction data were collected on a Synergy-R (Rigaku Oxford Diffraction) diffractometer equipped with a micro-focus Cu Kα radiation source (λ = 1.5418 Å), a hybrid pixel array detector (HPAD), and a low temperature system using cold nitrogen stream (100 K). Collected data were integrated, corrected, and scaled by the program CrysAlisPro. Empirical and numerical absorption corrections were applied in this process. All crystal structures were solved using SHELXT ver. 2018/2 (Sheldrick,

2015b) and refined using SHELXL ver. 2018/3 (Sheldrick, 2015a) programs. All the non-hydrogen atoms were refined anisotropically. All the hydrogen atoms were grown using the proper HFIX command and refined isotropically using the riding model. Compound **4** was obtained as small crystals and directly analyzed by an X-ray diffractometer, whereas compounds **3**, **5**–**7** were analyzed by the crystalline sponge method (Inokuma *et al*., 2013; Hoshino *et al*., 2016). The crystalline sponge (CS) $[(ZnCl_2)_3(tpt)_2 \cdot x(n\text{-hexane})]_n$ (tpt=2,4,6-tris(4-pyridyl)-1,3,5-triazine) was prepared according to the reported procedure (Sakurai *et al*., 2017).

3⊂CS: A 5 μL portion of a dimethoxyethane (DME) solution containing **3** (5 μg) was added to a microvial containing a CS and 45 μL of *n*-hexane. The vial was pieced with a needle and allowed to stand at 50°C for 1 day. Then, the CS was mounted on an X-ray diffractometer for the diffraction study.

5⊂CS: A 2 μL portion of a DME solution containing **5** (20 μg) was added to a microvial containing a CS and 18 μL of *n*-hexane. The vial was allowed to stand at 50°C for 3 days. Then, the CS was mounted on an X-ray diffractometer for the diffraction study.

6⊂CS: A 2 μL portion of a DME solution containing **6** (20 μg) was added to a microvial containing a CS and 18 μL of *n*-hexane. The vial was allowed to stand at 50°C for 3 days. Then, the CS was mounted on an X-ray diffractometer for the diffraction study.

7⊂CS: A 5 μL portion of a DME solution containing **7** (5 μg) was added to a microvial containing a CS and 45 μL of *n*-hexane. The vial was pieced with a needle and allowed to stand at 50°C for 1 day. Then, the CS was mounted on an X-ray diffractometer for the diffraction study.

CCDC 2243019–2243023 contains the supplementary crystallographic data for this paper. These data can be obtained free of charge via

http://www.ccdc.cam.ac.uk/conts/retrieving.html.

Antimicrobial activity

Bioassays to detect antimicrobial activity were performed according to the method described by Murata *et al*. (2020). To detect antifungal activity, droplets (100 μL) of a conidial suspension (5.0×10^4 conidia mL^{-1}) of pathogenic fungi in solutions containing 10, 30, 100, 300, and 1,000 μM of the compounds of interest and 1% dimethyl sulfoxide (DMSO) were placed on a glass slide and incubated at 25°C in the dark. The conidia were inspected under a microscope (BX43; Olympus, https: //www.olympuslifescience.com/en/) to count the number of germinated conidia and to measure the length of the germ tube using Image J (https: //imagej.nih.gov/ij/docs/install/windows.html). To detect antibacterial activity, bacterial suspensions (10 μL) were inoculated into 190 μL of medium containing 0, 10, 30, 100, 300, or 1,000 μM of each compound in microtubes. The microtubes were incubated at 25°C with shaking for 21 h (for *Burkholderia glumae*) and 18 h (for *Xanthomonas oryzae*), and the optical density at 600 nm (OD_{600}) was determined using an Infinite200 PRO plate reader (Tecan, https: //www.tecan.com/).

Analysis of phytoalexins

The leaf extract was subjected to LC-MS/MS analysis in MRM mode. The LC conditions were as follows: column: Acquity UPLC BEH C18 column (2.1 × 50 mm, 1.7 μm) (Waters); flow rate: 0.2 mL min^{-1}; column temperature: 40°C; solvents: 0.1% aqueous formic acid (A) and 0.1% formic acid in acetonitrile (B); gradient: 36–70% B/(A + B) (10 min). Compounds were analyzed in positive ion mode with nitrogen as the

collision gas. The monitored precursor-to-product transitions are described in Supplementary Table S3.3. A methanol solution of authentic compounds at 20 μg mL^{-1} was used as an external standard. The detection limits for phytoalexins with our analytical system is summarized in Supplementary Table S3.3.

Chapter 4
General Discussion

In this study, we found natural variation of diterpenoid phytoalexin production in *O. sativa*. It is likely that the intraspecific diversity in wild rice was inherited by cultivated rice. Previously, Murata *et al*. (2020) and Kariya *et al*. (2019) found that the cause of natural variation in sakuranetin and oryzalexin accumulation is in the expression and/or enzymatic activity of the biosynthetic enzymes. Analyses of the biosynthetic genes would address the causes leading to these variations in phytoalexin accumulation. Furthermore, because natural variation reflects the process by which organisms adapt to their habitats, identifying and analyzing the genes responsible for natural variation will provide insight into the process of adaptive evolution.

A majority of *O. sativa* and *O. rufipogon* strains accumulated momilactone A and phytocassanes A, D, and G. Cultivars that accumulated smaller amounts of momilactones and phytocassanes tended to accumulate abietoryzins (Figures 3.3b and 3.3c). This conserved accumulation of diterpenoid phytoalexins suggests their critical roles in their survival. However, in many cultivars, individual phytoalexin concentrations appeared to be insufficient to exert their antifungal activity. These phytoalexins may function in an additive or synergistic manner, and therefore, the total concentration of phytoalexins is important. Other bioactivities of phytoalexins aside from antimicrobial activity have also been reported. For example, momilactone B is secreted by the roots and has an allelopathic effect on other plants (Kato-Noguchi, 2004). The accumulation of diterpenoid phytoalexins affects the resistance to the root-knot nematode, *Meloidogyne graminicola*, and the ratio of the nematode species, such as *Acrobeloides* and

Meloidogyne, in the rice roots and its rhizosphere (Desmedt *et al*., 2022). Lu *et al*. (2018) reported that the rhizosphere microbiota in phytoalexin-deficient rice mutants was altered from those in wild type. Because of this ecological multifunctionality, the accumulation of various phytoalexins might have been beneficial for rice species to adapt to changing biological environments at some stages in evolution. Rice expanded their habitat to various regions with diverse climate and soil conditions, and thus, was likely exposed to changes in the biotic environment. The utilization of multiple antimicrobial compounds and their flexible composition may contribute to the robustness of rice as a species against various pests in a wide habitat.

We added seven undescribed diterpenoid compounds to the large list of phytoalexins in rice. The reason for this multiplicity of phytoalexin production in rice is not clear. It has been demonstrated that the amounts of duplicated genes have been correlated to the variation in habitat. In *Drosophila* species, the proportion of duplicated genes in the whole genome is correlated with the size of the climate envelope estimated by bioclimatic variables (Makino and Kawata, 2012). A study of the genomes of euarchontoglires showed that species in variable environments have more small-scale duplication (SSD) genes than species in habitats with low variation, a result suggesting that SSD genes are important for adapting to novel environments and surviving environmental changes (Tamate *et al*., 2014). Analogously, the duplication and diversification of biosynthetic genes for phytoalexin production may be beneficial to deal with various biological stresses in various habitats.

Chapter 5

Conclusion

As shown in chapter 2, we examined the natural variation in diterpenoid phytoalexin production in rice and found that the amount of oryzalexin A, momilactones and phytocassanes greatly varies depending on the cultivar. The cultivars and strains that showed oryzalexin A accumulating chemotype were minority. On the other hand, momilactones and phytocassanes were accumulated in 68 cultivars and 64 cultivars, respectively among 69 cultivars in WRC. In addition, we identified two undescribed phytoalexins, oryzalactone and phytocassane G. Only three cultivars in the WRC showed the oryzalactone-accumulating chemotype, whereas all cultivars except for WRC11 showed the phytocassane G-accumulating chemotype. The natural variation in phytoalexin accumulation in cultivated rice is considered to be a reflection of the diversity of phytoalexin accumulation in the ancestral wild species *O. rufipogon*.

In chapter 3, we identified new phytoalexins, abietoryzins, from the 'Jinguoyin', which does not accumulate known diterpenoid phytoalexins. The analysis of the abietoryzins in various rice cultivars indicated that they are one of the major phytoalexin groups in rice because they were detected in 30 of 69 cultivars in WRC. This finding of a previously underreported major group of phytoalexins emphasizes the importance of analyzing chemodiversity in a species. In addition, the present study expands the diversity of the carbon skeletons of rice phytoalexins. The characterization of the diterpene synthase responsible for the formation of the carbon skeleton of abietoryzins is important for understanding the evolution of diterpenoid phytoalexins in rice.

References

Akagi, A., Fukushima, S., Okada, K., Jiang, C.J., Yoshida, R., Nakayama, A., Shimono, M., Sugano, S., Yamane, S., Takatsuji, A., 2014. WRKY45-dependent priming of diterpenoid phytoalexin biosynthesis in rice and the role of cytokinin in triggering the reaction. *Plant Molecular Biology* **86**, 171-183.

Akatsuka, T., Kodama, O., Kato, H., Kono, Y., Takeuchi, S., 1983. 3-Hydroxy-7-oxo-sandaraco-pimaradiene (oryzalexin A), a new phytoalexin isolated from rice blast leaves. *Agricultural and Biological Chemistry* **47**, 445–447.

Akatsuka, T., Kodama, O., Sekido, H., Kono, Y., Takeuchi S., 1985. Novel phytoalexins (oryzalexins A, B and C) isolated from rice blast leaves infected with *Pyricularia oryzae*. *Agricultural and Biological Chemistry* **49**, 1689–1694.

Cartwright, D.W., Langcake, P., Pryce, R.J., Leworthy, D.P., Ride, J.P., 1981. Isolation and characterization of two phytoalexins from rice as momilactones A and B. *Phytochemistry* **20**, 535–537.

Czechowski, T., Larson, R.T., Catania, M.Y., Harvey, D., Wei, C., Essome, M., Brown, D. G., Graham, A.I., 2018. Detailed phytochemical analysis of high- and low artemisinin-producing chemotypes of *Altemisia annua*. *Front. Plant Sci.* **9**, 641.

Deng, M., Zhang, X., Luo, J., Liu, H., Wen, W., Luo, H., Yan, J., Xiao, Y., 2020. Metabolomics analysis reveals differences in evolution between maize and rice. *Plant J*.

103, 1710–1722.

Desmedt, W., Kudjordjie, N.E., Chavan, N.S., Zhang, J., Li, R., Yang, B., Nicolaisen, M., Mori, M., Peters, J.R., Vanholme, B., Vestergard, M., Kyndt, T., 2022. Ride diterpenoid phytoalexins are involved in defence against parasitic nematodes and shape rhizosphere nematode communities. *New Phytol.* **235**, 1231–1245.

FAO, 2010. Appendix 2, Major germplasm collections by crop and institute. The second report on the state of the world's plant genetic resources for food and agriculture. *Rome*, 241–283.

Forman, V., Callari, R., Folly, C., Heider, H., Hamberger, B., 2017. Production of putative diterpene carboxylic acid intermediates of triptolide in yeast. *Molecules* **22**, 981.

Gao, W., Hillwig, L.M., Huang, L., Cui, G., Wang, X., Kong, J., Yang, B., Peters, J.R., 2009. A functional genomics approach to tanshinone biosynthesis provides stereochemical insights. *Org. Lett.* **11**, 5170–5173.

Horie, K., Inoue, Y., Sakaki, M., Yao, Q., Tanimoto, Y., Koga, J., Toshima, K., Hasegawa, M., 2015. Identification of UV-Induced diterpenes including a new diterpene phytoalexin, phytocassane F, from rice leaves by complementary GC/MS and LC/MS approaches. *Journal of Agricultural and Food Chemistry* **63**, 4050–4059.

Hoshino, M., Khutia, A., Xing, H., Inokuma, Y., Fujita, M., 2016. The crystalline sponge

method updated. *IUCrJ* **3**, 139–151.

Huang, X., Kurata, N., Wei, X., Wang, Z., Aho-Wang, A., Zhao, Q., Zhao, Y., Liu, K., Lu, H., Li, W. et al., 2012. A map of rice genome variation reveals the origin of cultivated rice. *Nature* **490**, 497–501.

Huffaker, A., Kaplan, F., Vaughan, M.M., Dafoe, N.J., Ni, X., Rocca, J.R., Alborn, H.T., Teal, P.E.A., Schmelz, E., 2011. A novel acidic sesquiterpenoids constitute a dominant class of pathogen-induced phytoalexins in maize. *Plant Physiology* **156**, 2082–2097.

Inokuma, Y., Yoshioka, S., Ariyoshi, J., Arai, T., Hirota, Y., Takada, K., Matsunaga, S., Rissanen, K., Fujita, M., 2013. X-ray analysis on the nanogram to microgram scale using porous complexes. *Nature* **495**, 461–466.

Inoue, Y., Sakai, M., Yao, Q., Tanimoto, Y., Toshima, H., Hasegawa, M., 2013. Identification of a novel casbane-type diterpene phytoalexin, *ent*-10-oxodepressin, from rice leaves. *Biosci. Biotechnol. Biochem.* **77**(4), 760–765.

Ishihara, A., Kumeda, R., Hayashi, N., Yagi, Y., Sakaguchi, N., Kokubo, Y., Ube, N., Tebayashi, S., Ueno, K., 2017. Induced accumulation of tyramine, serotonin, and related amines in response to *Bipolaris sorokiniana* infection in barley. *Biosci. Biotechnol. Biochem.* **81**, 1090–1098.

Jiang, Z.-P., Tian, L.-W., Shen, L., Wu, J., 2018. Ent-abietanes from the Godavari

mangrove, *Ceriops decandra*: absolute configuration and NF-κB inhibitory activity. *Fitoterapia* **130**, 272–280.

Kanno, Y., Otomo, K., Kenmoku, H., Mitsuhashi, W., Yamane, H., Oikawa, H., Toshima, H., Matsuoka, M., Sassa, T., Toyomasu, T., 2006. Characterization of a rice gene family encoding type-A diterpene cyclase. *Biosci. Biotechnol. Biochem.* **70**, 1702–1710.

Kariya, K., Murata, K., Kokubo, Y., Ube, N., Ueno, K., Yabuta, Y., Teraishi, M., Okumoto, Y., Mori, N., Ishihara, A., 2019. Variation of diterpenoid phytoalexin oryzalexin A production in cultivated and wild rice. *Phytochemistry* **166**, 112057.

Kato, H., Kodama, O., Akatsuka, T., 1993. Oryzalexin E, a diterpene phytoalexin from UV-irradiated rice leaves. *Phytochemistry* **33**, 79–81.

Kato, H., Kodama, O., Akatsuka, T., 1994. Oryzalexin F, a diterpene phytoalexin from UV-irradiated rice leaves. *Phytochemistry* **36**, 299–301.

Kato-Noguchi, H., 2004. Allelopathic substance in rice root exudates: rediscovery of momilactone B as an allelochemical. *Plant Physiol.* **161**, 271–276.

Kliebenstein D. J., Kroymann J., Brown P., Figuth A., Pedersen D., Gershenzon J., Mitchell-Olds T., 2001. Genetic control of natural variation in *Arabidopsis* glucosinolate accumulation. *Plant physiol.* **126**(2), 811–825.

Kodama, O., Miyakawa, J., Akatsuka, T., Kiyosawa, S., 1992a. Sakuranetin, a flavanone phytoalexin from ultraviolet-irradiated rice leaves. *Phytochemistry* **31**, 3807–3809.

Kodama, O., Li, W.X., Tamogami, S., Akatsuka, T., 1992b. Oryzalexin S, a novel stemarane-type diterpene rice phytoalexin. *Biosci. Biotechnol. Biochem.* **56**, 1002–1003.

Koga, J., Shimura, M., Oshima, K., Ogawa, N., Yamauchi, T., Ogasawara, N., 1995. Phytocassanes A, B, C and D, novel diterpene phytoalexins from rice, *Oryza sativa* L. *Tetrahedron* **51**, 7907–7918.

Koga, J., Ogawa, N., Yamauchi, T., Kikuchi, M., Ogasawara, N., Shimura, M., 1997. Functional moiety for the antifungal activity of phytocassane E, a diterpene phytoalexin from rice. *Phytochemistry* **44**, 249–253.

Kojima, Y., Ebana, K., Fukuoka, S., Nagamine, T., Kawase, M., 2005. Development of an RFLP-based rice diversity research set of germplasm. *Breed Sci.* **55**, 431–440.

Kono Y., Takeuchi S., Kodama O., Akatsuka T., 1984. Absolute configuration of oryzalexin A and structures of its related phytoalexins isolated from rice blast leaves infected with *Pyricularia oryzae*. *Agricultural and Biological Chemistry* **48**(1), 253-255.

Kroymann, J., Donnerhacke, S., Schnabelrauch, D., Mlichell, O.T., 2003. Evolutionary dynamics of an *Arabidopsis* insect resistance quantitative trait locus. *PNAS* **100** (suppl_2), 14587–14592.

Li G., Xu Q., He C., Zeng L., Wang H., 2014. Two new anti-fungal diterpenoids from the husks of *Oryza sativa*. *Phytochemistry Letters* **10**, 309–312.

Li, R., Zhang, J., Li, Z., Peters, J.R., Yang, B., 2022. Dissecting the labdane-related diterpenoid biosynthetic gene clusters in rice reveals directional cross-cluster phytotoxicity. *New Phytol.* **233**, 878–889.

Lu, X., Zhang, J., Brown, B., Li, R., Rodriguez-Romero, J., Berasategui, A., Liu, B., Xu, M., Luo, D., Pan, Z. *et al*., 2018. Inferring roles in defense from metabolic allocation of rice diterpenoids. *Plant Cell* **30**, 1119–1131.

Makino, T., Kawata, M., 2012. Habitat variability correlates with duplicate content of *Drosophila* genomes. *Mol. Biol. Evol.* **29**, 3169–3179.

Mayama, S., Matsuura, Y., Iida, H., Tani, T., 1982. The role of avenalumin in the resistance of oat to crown rust, *Puccinia coronata* f. sp. *Avenae*. *Physiological Plant Pathology* **20**, 189–199.

Miyagawa, H., Ishihara, A., Nishimoto, T., Ueno, T., Mayama, S., 1995. Induction of avenanthramides in oat leaves inoculated with crown rust fungus, *Puccinia coronata* f. sp. *Avenae*. *Biosci. Biotechnol. Biochem.* **59**, 2305–2306.

Miyamoto, K., Fujita, M., Matthew, S.R., Akashi, S., Sugawara, C., Sakai, A., Horie, K.,

Hasegawa, M., Kawaide, H., Mitsuhashi, W. *et al*., 2016. Evolutionary trajectory of phytoalexin biosynthetic gene clusters in rice. *Plant J.* **87**, 293–304.

Morimoto, N., Ueno, K., Teraishi, M., Okumoto, Y., Mori, N., Ishihara, A., 2018. Induced phenylamide accumulation in response to pathogen infection and hormone treatment in rice (*Oryza sativa*). *Biosci. Biotechnol. Biochem.* **82**, 407–416.

Murata, K., Kitano, T., Yoshimoto, R., Takata, R., Ube, N., Ueno, K., Ueno, M., Yabuta, Y., Teraishi, M., Holland, K.C. *et al*., 2020. Natural variation in the expression and catalytic activity of a naringenin 7-*O*-methytransferase influences antifungal defenses in diverse rice cultivars. *Plant J.* **101**, 1103–1117.

Nomura, T., Ishihara, A., Iwamura, H., Endo, R.T., 2007. Molecular characterization of benzoxazinone-deficient mutation in diploid wheat. *Phytochemistry* **68**, 1008–1016.

Otomo, K., Kenmoku, H., Oikawa, H., Konig, W.A., Toshima, H., Mitsuhashi, W., Yamane, H., Sassa, T., Toyomasu, T., 2004. Biological functions of *ent*- and *syn*-copalyl diphosphate synthases in rice: key enzymes for the branch point of gibberellin and phytoalexin biosynthesis. *Plant J*. **39**, 886–893.

Pena, D.L.R., Sattely, S.E., 2021. Re-routing plant terpene biosynthesis enables momilactone pathway elucidation. *Nat. Chem. Biol.* **17**, 205–212.

Perrin D.R. and Bottomley, W., 1962. Studies on phytoalexins. V. The structure of pisatin

from Pisum sativum L. *J. AM. Chem. Soc.* **84**, 1919–1922.

Sakamoto, T., Miura, K., Itoh, H., Tatsumi, T., Ueguchi-Tanaka, M., Ishiyama, K., Kobayashi, M., Agrawal, G.K., Takeda, S., Abe, K., Miyao, A., Hirochika, H., Kitano, H., Ashikari, M., Matsuoka, M., 2004. An overview of gibberellin metabolism enzyme genes and their related mutants in rice. *Plant Physiol.* **134**, 1642–1653.

Sakurai, F., Khutia, A., Kikuchi, T., Fujita, M., 2017. X-ray structure analysis of Ncontaining nucleophilic compounds by the crystalline sponge method. *Chem. Eur J.* **23**, 15035–15040.

Schmelz, E.A., Kaplan, F., Huffaker, A., Dafoe, N.J., Vaughan, M.M., Ni, X., Rocca, J.R., Alborn, H.T., Teal, P.E.A., 2011. Identity, regulation, and activity of inducible diterpenoid phytoalexins in maize. *PNAS*, **108**, 5455–5460.

Sekido, H., Endo, T., Suga, R., Kodama, O., Akatsuka, T., Kono, Y., Takeuchi, S., 1986. Oryzalexin D (3, 7-Dihydroxy-(+)-sandaracopimaradiene), a new phytoalexin isolated from blast-infected rice leaves. *Pesticide Science*, **11**, 369–372.

Sheldrick, G.M., 2015a. Crystal structure refinement with SHELXL. *Acta Crystallogr. Sect. C-Struct. Chem.* **71**, 3–8.

Sheldrick, G.M., 2015b. Shelxt - integrated space-group and crystal-structure determination. *Acta Crystallogr. Sect. A-Found. Adv.* **71**, 3–8.

Stein, J.C., Yu, Y., Copetti, D., Zwickl, D.J., Zhang, L., Zhang, C., Chougule, K., Gao, D., Iwata, A., Goicoechea, J.L. *et al*., 2018. Genomes of 13 domesticated and wild rice relatives highlight genetic conservation, turnover and innovation across the genus *Oryza*. *Nat. Genet.* **50**, 285–296.

Tamate, C.S., Kawata, M., Makino, T., 2014. Contribution of nonohnologous duplicated genes to high habitat variability in mammals. *Mol. Biol. Evol.* **31**, 1779–1786.

Toyomasu, T., Usui, M., Sugawara, C., Otomo, K., Hirose, Y., Miyao, A., Hirochika, H., Okada, K., Shimizu, T., Koga, J., Hasegawa, M., Chuba, M., Kawana, Y., Kuroda, M., Minami, E., Mitsuhashi, W., Yamane, H., 2014. Reverse-genetic approach to verify physiological roles of rice phytoalexins: characterization of a knockdown mutant of OsCPS4 phytoalexin biosynthetic gene in rice. *Physiol Plant* **150**, 55–62.

Toyomasu, T., Miyamoto, K., Shenton, R.M., Sakai, A., Sugawara, C., Horie, K., Kawaide, H., Hasegawa, M., Chuba, M., Mitsuhashi, W., Yamane, H., Kurata, N., Okada, K., 2016. Characterization and evolutionary analysis of *ent*-kaurene synthase like genes from the wild rice species *Oryza rufipogon*. *Biochem. Biophys. Res. Commun.* **480**, 402–408.

Toyomasu, T., Shenton, M.R., Okada, K., 2020. Evolution of labdane-related diterpene synthases in cereals. *Plant and Cell Physiol.* **61**, 1850–1859.

Vaughan, D.A. 1991. Choosing rice germplasm for evaluation. *Euphytica* **54**, 147–154.

Wang, S., Alseekh, S., Fernie, A.R., Luo, J., 2019. The structure and function of major plant metabolite modifications. *Molecular Plant*, **12**(7), 899–919.

Wang, Z., Peters, J.R., 2022. Tanshinones: leading the way into Lamiaceae labdane-related diterpenoid biosynthesis. *Curr. Opin. Plant Biol.* **66**, 102189.

Xu, M., Wilderman, R.P., Morrone, D., Xu, J., Roy, A., Margis-Pinheiro, M., Upadhyaya, M.N., Coates, M.R., Peters, J.R., 2007. Functional characterization of the rice kaurene synthase-like gene family. *Phytochemistry* **68**, 312–326.

Ye, Z., Yamazaki, K., Minoda, H., Miyamoto, K., Miyazaki, S., Kawaide, H., Yajima, A., Nojiri, H., Yamane, H., Okada, K., 2018. *In planta* functions of cytochrome P450 monooxygenase genes in the phytocassane biosynthetic gene cluster on rice chromosome 2. *Biosci. Biotechnol. Biochem.* **82**, 1021–1030.

Zhang, J., Li, R., Xu, M., Hoffmann, I.R., Zhang, Y., Liu, B., Zhang, M., Yang, B., Li, Z., Peters, J.R., 2021. A (conditional) role for labdane-related diterpenoid natural products in rice stomatal closure. *New Phytol.* **230**, 698–709.

Zhang, Z., Zhang, F., Deng, Y., Sun, L., Mao, M., Chen, R., Qiang, Q., Zhou, J., Long, T., Zhao, X., Liu, X., Wang, S., Yang, J., Luo, J., 2022. Integrated metabolomics and transcriptomics analyses reveal the metabolic differences and molecular basis of

nutritional quality in landraces and cultivated rice. *Metabolites* **12**, 284.

Zi, J., Peters, J.R., 2013. Characterization of CYP76AH4 clarifies phenolic diterpenoid biosynthesis in the Lamiaceae. *Org. Biomol. Chem.* **11**, 7650–7652.

Zust, T., Heichinger, C., Grossniklaus, U., Harrington, R., Kliebenstein, J.D., Turnbull, A.L., 2012. Natural enemies drive geographic variation in plant defenses. *Science* **338**, 116–119.

Acknowledgement

I express my gratitude and sincere appreciation to my respected supervisor, Professor Atsushi Ishihara, Tottori University, for his kind and warm guiding.

I also express my appreciation to associate professor Kotomi Ueno of Tottori University for her advice and support.

I would like to thank the collaborators for their invaluable assistance in helpful advice and providing plants, pathogens, and genetic materials.

I am grateful to members of Naturel Products Chemistry laboratory, Tottori university, for their technical assistance.

Finally, I am grateful to my family for encouragement and support.

Summary

Cultivated rice (*Oryza sativa*) accumulates antimicrobial compounds, phytoalexins, in response to pathogen infection. About 20 compounds have been reported as phytoalexins from cultivated rice, most of them are diterpenoid. Phytoalexins play an important role in the biological defense. In this study, we focused on the intraspecific diversity of diterpenoid phytoalexin production in rice.

World Rice Core Collection (WRC) is a group of cultivars selected from *O. sativa* cultivars collected from various regions in the world. The accumulation of five representative diterpenoid phytoalexins was examined in the UV-irradiated WRC leaves. Only 12 cultivars in WRC accumulated oryzalexin A, while the majority of the cultivars accumulated momilactones and phytocassanes. These findings indicated the intraspecific diversity in the accumulation of diterpenoid phytoalexins in *O. sativa*. The accumulation of oryzalexin A in the wild rice *O. rufipogon*, the ancestor of cultivated rice, and the accumulation of momilactones and phytocassanes in several *Oryza* species including *O. rufipogon* were examined. Intraspecific diversity in phytoalexin accumulation was found in wild rice species. These results suggested that intraspecific diversity in phytoalexin production occurs in the wild rice and that this trait is retained in the cultivated rice *O. sativa*.

During the analysis of momilactone A, two unknown compounds, presumed to be momilactone A isomers, were detected in the extracts from 'Jaguary' and 'Basilanon'. Each compound was isolated from rice leaves irradiated with UV-light. Both compounds were induced by the infection of rice blast fungus and showed antimicrobial activity against pathogenic fungi. Therefore, these compounds were regarded as new phytoalexins in rice, and were named as oryzalactone and phytocassane G based on their chemical

structures. While oryzalactone was accumulated only in three WRC cultivars, phytocassane G was accumulated in all cultivars except 'Jinguoyin'. In wild rice species, oryzalactone accumulated in limited number of strains of AA genome species, while phytocassane G accumulated in almost all strains of AA genome species.

Some strains in the WRC showed low accumulation of diterpenoid phytoalexins. Among them, 'Jinguoyin' did not accumulate any analyzed diterpenoid phytoalexins. Because phytoalexins play a crucial role in disease resistance, it is presumed that this cultivar accumulated different phytoalexins in response to pathogen attack. In this context, the presence of compounds that specifically accumulate in *Bipolaris oryzae*-infected leaves was examined by LC-MS analysis. Five compounds were found to accumulate in the leaves and were isolated and identified. These five compounds were diterpenoids with benzene rings and named abietoryzins A–E because they were first isolated from pathogen infected rice leaves. They inhibited conidia germination or germ tube elongation of *Pyricularia oryzae* and *B. oryzae*, indicating that they function as phytoalexins.

The cultivars that accumulate lower levels of momilactones and phytocassanes tended to accumulate high levels of abietoryzins in response to UV-light irradiation. Thirty of the 69 WRC cultivars accumulated at least one abietoryzin. In addition, the accumulated amounts of abietoryzins were largest among the analyzed phytoalexins in 15 cultivars. Thus, abietoryzins are one of the major groups of phytoalexins in rice although their occurrence has been overlooked to date.

Comparison of phytoalexin accumulation in wide range of cultivars revealed intraspecific diversity in their accumulation. The discovery of novel phytoalexins indicated the importance of comparative analysis of multiple cultivars. To better understand the process of diversification of diterpenoid phytoalexin production in genus

Oryza, it is important to identify and characterize genes responsible for differences in phytoalexin accumulation.

摘要

栽培イネ（*Oryza sativa*）は、病原菌の感染に応答して抗菌性化合物、ファイトアレキシン、を蓄積する。栽培イネからは約 20 種の化合物がファイトアレキシンとして報告されているが、そのほとんどはジテルペノイド化合物である。これらの化合物群は、イネの生体防御に重要な役割を果たしている。この研究では、イネにおいてジテルペノイドファイトアレキシン生産に種内多様性があるか明らかにすることを目的とした。

世界各地の栽培イネから選抜された、来歴情報と対立遺伝子の多様性を広くカバーした品種群、世界のイネ コアコレクション (WRC) 69 品種を用いて、紫外線照射葉における 5 種のジテルペノイドファイトアレキシンの蓄積量を調べた。オリザレキシン A は WRC の中で 12 品種しか蓄積しなかったが、モミラクトン類およびファイトカサン類はほとんどの品種が蓄積していた。この分析により、栽培イネにおいてジテルペノイドファイトアレキシンの蓄積に関する種内多様性があることが示された。つづいて、同様の方法で、栽培イネの祖先野生イネ *O. rufipogon* におけるオリザレキシン A の蓄積量と、*O. rufipogon* を含む複数の *Oryza* 属植物におけるモミラクトン類およびファイトカサン類の蓄積量を調べた。分析したいずれの化合物も、栽培イネと同様に、野生イネにおいてもそれらの蓄積に関する種内多様性が見出された。これらの結果から、ファイトアレキシン生産の種内多様性は野生イネにも存在しており、これが栽培イネ *O. sativa* にも受け継がれているものと推察された。

モミラクトン A の分析の過程で、‘Jaguary’と‘Basilanon’のそれぞれからモミラクトン A 類縁体と推定される 2 種の化合物を見出した。それぞれの化合物を紫外線照射したイネの葉から単離した。各種機器分析によりその構造を同定したところ、いずれの化合物も未報告であったことから、それぞれオリザラクトンおよびファイトカサン G と名付けた。いずれの化合物も、イネいもち病菌の感染によりその蓄積が誘導され、イネいもち病菌に対して抗菌活性を示したことから、イネの新規ファイトアレキシンであると結論し

た。オリザラクトンは、WRC の中がでは、3品種しか存在しなかったが、ファイトカサン G は‘Jinguoyin’を除く全ての品種が蓄積した。野生イネにおいても、オリザラクトンは AA ゲノム種の限られた系統しか蓄積しなかった一方で、ファイトカサン G は AA ゲノム種のほとんど全ての系統が蓄積していた。

WRC にはジテルペノイドファイトアレキシンの蓄積量が少ない系統があった。特に、‘Jinguoyin’は、分析したいずれのジテルペノイドファイトアレキシンを蓄積しなかった。ファイトアレキシンはイネの生体防御において重要であることから、‘Jinguoyin’は他の品種とは異なる化合物をファイトアレキシンとして蓄積する可能性が想定された。そこで、‘Jinguoyin’にイネごま葉枯病菌を接種し、感染葉特異的に蓄積する化合物を LC-MS 分析により探索した。その結果、5 種の化合物が見出された。これらの化合物を単離・同定したところ、いずれもベンゼン環を有するジテルペノイドだった。これらは、病原菌が感染したイネから初めて単離されたため、アビエトリジン A–E と名付けた。糸状菌であるイネいもち病菌とイネごま葉枯病菌の胞子発芽、あるいは、発芽管の伸長を阻害したことから、ファイトアレキシンとして機能していると考えられた。

紫外線照射葉において、モミラクトン類およびファイトカサン類の蓄積量が少ない品種では、アビエトリジン類が高濃度に蓄積する傾向があった。WRC 69 品種のうち、30 品種が少なくとも 1 種のアビエトリジン類を蓄積した。また、15 品種では分析したファイトアレキシンの中でアビエトリジン類の蓄積量が最も高かった。したがって、アビエトリジン類は、これまで見過ごされてきたものの、イネのファイトアレキシンの主要なグループであるとことがわかった。

多数の栽培イネのファイトアレキシンの蓄積量の比較により、その蓄積に関する種内多様性を発見した。新たなファイトアレキシンを複数発見できたことから、多系統の比較分析の重要性が示された。イネ属におけるジテルペノイドファイトアレキシン生産の多様化の過程をより深く理解するために、ファイトアレキシンの生合成遺伝子やその

発現制御に関わる因子の同定が重要であると考えられる。

List of publications

Chapter 2

Kariya, K., Ube, N., Ueno, M., Teraishi, M., Okumoto, Y., Mori, N., Ueno, K. and Ishihara, A. (2020) Natural variation of diterpenoid phytoalexins in cultivated and wild rice species. *Phytochemistry* 180, 112518.

Chapter 3

Kariya, K., Fujita, A., Ueno, M., Yoshikawa, T., Teraishi, M., Taniguchi, Y., Ueno, K. and Ishihara, A. (2023) Natural variation of diterpenoid phytoalexins in rice: Aromatic diterpenoid phytoalexins in specific cultivars. *Phytochemistry* 211, 113708.

Supplementary materials

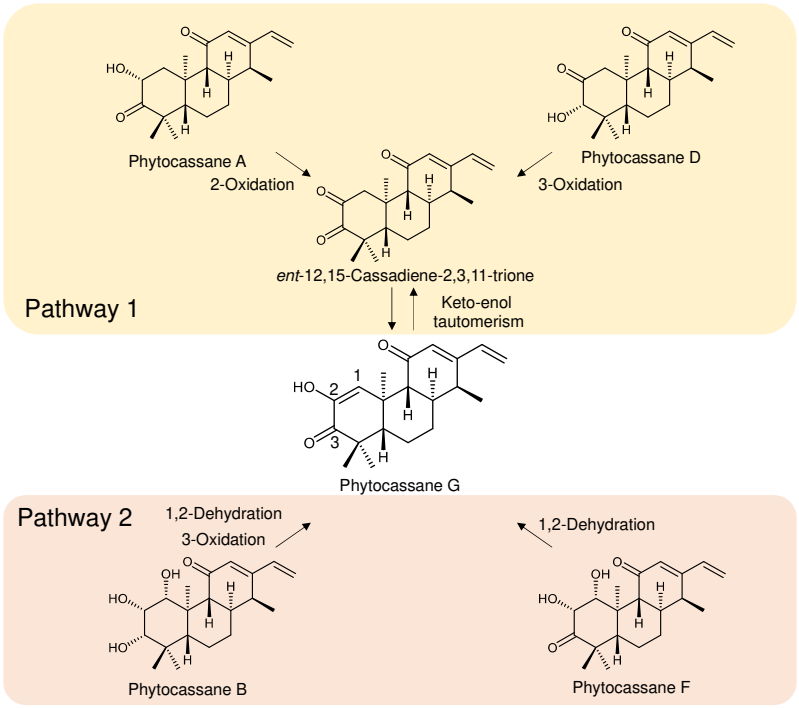

Supplementary Figure 2.1. Hypothetical biosynthesis pathways for phytocassane G. In pathway 1, phytocassanes A and D are precursors of phytocassane G, whereas in pathway 2, phytocassanes B and F are precursors.

Supplementary Table S2.1. Cultivars in the world rice core collection.

Number	Cultivar	Country	Subspecies*
WRC01	Nipponbare	Japan	TEJ
WRC02	Kasalath	India	IND
WRC03	Bei Khe	Cambodia	IND
WRC04	Jena 035	Nepal	IND
WRC05	Naba	India	IND
WRC06	Puluik Arang	Indonesia	IND
WRC07	Davao 1	Philippines	IND
WRC09	Ryou Suisan Koumai	China	IND
WRC10	Shuusoushu	China	IND
WRC11	Jinguoyin	China	IND
WRC12	Dahonggu	China	IND
WRC13	Asu	Bhutan	IND
WRC14	IR 58	Philippines	IND
WRC15	Co 13	India	IND
WRC16	Vary Futsi	Madagascar	IND
WRC17	Keiboba	China	IND
WRC18	Qingyu	Taiwan	IND
WRC19	Deng Pao Zhai	China	IND
WRC20	Tadukan	Philippines	IND
WRC21	Shwe Nang Gyi	Myanmar	IND
WRC22	Calotoc	Philippines	-
WRC23	Lebed	Philippines	-
WRC24	Pinulupot 1	Philippines	-
WRC25	Muha	India	IND
WRC26	Jhona 2	India	IND
WRC27	Nepal 8	Nepal	IND
WRC28	Jarjan	Bhutan	IND
WRC29	Kalo Dhan	Nepal	IND
WRC30	Anjana Dhan	Nepal	IND
WRC31	Shoni	Bangladesh	IND
WRC32	Tupa 121-3	Bangladesh	IND
WRC33	Surjamukhi	India	IND
WRC34	ARC 7291	India	IND
WRC35	ARC 5955	India	IND

WRC36	Ratul	India	IND
WRC37	ARC 7047	India	IND
WRC38	ARC 11094	India	IND
WRC39	Badari Dhan	Nepal	IND
WRC40	Nepal 555	India	IND
WRC41	Kaluheenati	Sri Lanka	IND
WRC42	Local Basmati	India	IND
WRC43	Dianyu 1	China	TEJ
WRC44	Basilanon	Philippines	IND
WRC45	Ma sho	Myanmar	TRJ
WRC46	Khao Nok	Laos	TRJ
WRC47	Jaguary	Brazil	TRJ
WRC48	Khau Mac Kho	Vietnam	TRJ
WRC49	Padi Perak	Indonesia	TRJ
WRC50	Rexmont	USA	TRJ
WRC51	Urasan 1	Japan	TRJ
WRC52	Khau Tan Chiem	Vietnam	TRJ
WRC53	Tima	Bhutan	TRJ
WRC55	Tupa729	Bangladesh	TRJ
WRC57	Milyang 23	Korea	IND
WRC58	Neang Menh	Cambodia	IND
WRC59	Neang Phtong	Cambodia	IND
WRC60	Hakphaynhay	Laos	IND
WRC61	Radin Goi Sesat	Malaysia	IND
WRC62	Kemasin	Malaysia	IND
WRC63	Bleiyo	Thailand	IND
WRC64	Padi Kuning	Indonesia	IND
WRC65	Rambhog	Indonesia	IND
WRC66	Bingala	Myanmar	IND
WRC67	Phulba	India	TEJ
WRC68	Khao Nam Jen	Laos	TEJ
WRC97	Chin Galay	Myanmar	IND
WRC98	Deejiaohualuo	China	IND
WRC99	Hong Cheuh Zai	China	IND
WRC100	Vandaran	Sri Lanka	IND

*TEJ: *temperate japonica*, TRJ: *tropical japonica*, IND: *indica*.

Supplementary Table S2.2. Wild rice strains used in this study.

Accession No.	Species	Country	Phylogenetic group*
W0120	*O. rufipogon*	India	*Or*-II
W0130	*O. rufipogon*	India	*Or*-I
W0138	*O. rufipogon*	India	*Or*-III
W0141	*O. rufipogon*	India	*Or*-III
W0170	*O. rufipogon*	Thailand	*Or*-I
W0593	*O. rufipogon*	Malaya	*Or*-III
W0596	*O. rufipogon*	Malaya	*Or*-II
W0610	*O. rufipogon*	Burma	*Or*-I
W0698	*O. barthii*	Guinea	
W1196	*O. glumaepatula*	Colombia	
W1230	*O. rufipogon*	Dutch New Guinea	*Or*-I
W1236	*O. rufipogon*	Australian New Guinea	*Or*-II
W1244	*O. rufipogon*	Nepal	*Or*-III
W1292	*O. rufipogon*	Indonesia	*Or*-II
W1294	*O. rufipogon*	Philippines	*Or*-III
W1295	*O. rufipogon*	Cambodia	*Or*-I
W1402	*O. brachyantha*	Sierra Leone	
W1432	*O. barthii*	Mali	
W1514	*O. punctata*	Kenya	
W1582	*O. punctata*	Tchad	
W1588	*O. barthii*	Cameroun	
W1590	*O. punctata*	Cameroun	
W1593	*O. punctata*	Nigeria	
W1643	*O. barthii*	Botswana	
W1703	*O. brachyantha*	Mali	
W1711	*O. brachyantha*	Cameroun	
W1715	*O. rufipogon*	China	*Or*-II
W1777	*O. rufipogon*	India	*Or*-III
W1798	*O. rufipogon*	Thailand	*Or*-II
W1807	*O. rufipogon*	Sri Lanka	*Or*-III
W1818	*O. rufipogon*	Bangladesh	*Or*-I
W1921	*O. rufipogon*	Thailand	*Or*-I
W1973	*O. rufipogon*	Indonesia	*Or*-III
W2052	*O. rufipogon*	Bangladesh	*Or*-II

W2078	*O. rufipogon*	Queensland, Australia	*Or*-III
W2112	*O. melidionalis*	Queensland, Australia	
W2113	*O. rufipogon* / *O. meridionalis*	Queensland, Australia	
W2115	*O. rufipogon* / *O. meridionalis*	Queensland, Australia	
W2117	*O. rufipogon* / *O. meridionalis*	Queensland, Australia	
W2140	*O. gluamepatula*	Brazil	
W2192	*O. glumaepatula*	Brazil	
W2299	*O. rufipogon*	Laos	*Or*-I
W2310	*O. rufipogon*	Laos	*Or*-II
TOG5495	*O. glaberrima*	Nigeria	
TOG5638	*O. glaberrima*	Nigeria	
TOG6800	*O. glaberrima*	Nigeria	
TOG6951	*O. glaberrima*	Nigeria	

* Huang *et al.* (2012) Nature **490**: 497-501.

Supplementary Table S2.3. Multiple reaction monitoring conditions and detection limits of phytoalexin analysis by liquid chromatography coupled with tandem mass spectrometry in MRM mode.

Compound	Precursor ion (*m*/*z*)	Product ion (*m*/*z*)	Cone voltage (V)	Collision energy (eV)	Detection limit (nmol g^{-1} FW)
Momilactone A	315.1	271.0	20	10	0.06
Momilactone B	331.1	269.1	20	14	0.20
Oryzalactone	315.2	271.2	20	15	0.12
Phytocassane A	317.2	299.2	20	10	0.45
Phytocassane D	317.2	299.2	20	10	0.40
Phytocassane G	315.1	297.1	20	10	0.40
Oryzalexin A	303.2	148.9	15	26	1.50

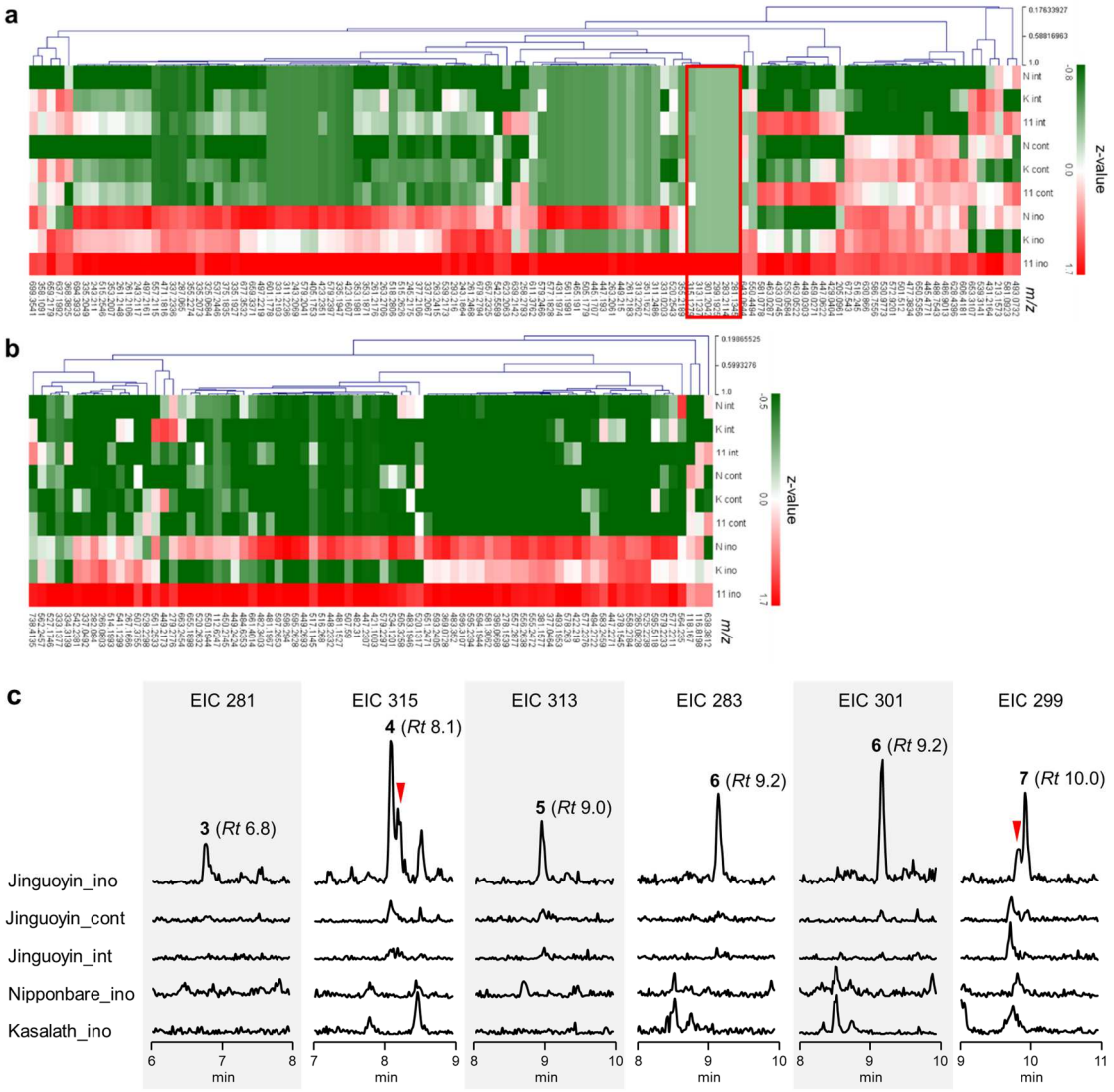

Supplementary Figure S3.1. Metabolic profiling of metabolites in the *Bipolaris oryzae*-infected leaves of rice cultivars: 'Nipponbare' (N), 'Kasalath' (K), and 'Jinguoyin' (11, WRC11). The conidia of *B. oryzae* were inoculated to rice leaves (ino). The leaves treated with water (control) and intact leaves (int) were also analyzed. Heat map of positive ions (**a**) and negative ions (**b**) were generated based on the means of average z-values of peak areas from three biological replicates. Ions of compounds accumulated only in 'Jinguoyin' were selected for further analysis. Extracted ion chromatograms (EIC) of the six selected ions in *Bipolaris oryzae* inoculated (ino) leaf extracts from 'Jinguoyin', 'Nipponbare', and 'Kasalath', and in intact (int) and control (con) leaf extracts from 'Jinguoyin' (**c**). The peaks indicated by the red arrows were ignored because they were not detected by the MarkerLynx analysis and were not induced by UV light irradiation. ino: inoculation, cont: control, and int: intact

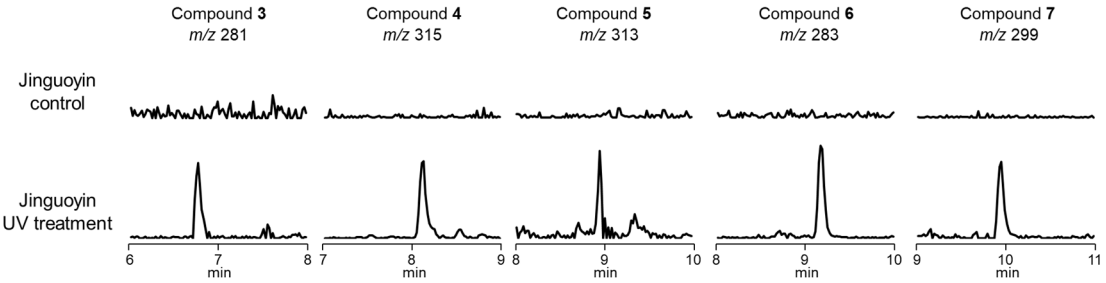

Supplementary Figure S3.2. Extracted ion chromatograms of compounds **3**–**7** in 'Jinguoyin' after UV light irradiation.

Crystallographic data for **3**⊂CS

Crystal size: 260 × 200 × 150 μm^3, refined formula: $C_{101.9}H_{111.5}Cl_{12}N_{24}O_{1.85}Zn_6$, formula weight (*Mr*) = 2519.66, colorless block, crystal system: Monoclinic, space group *C*2, *Z* = 4, 29824 unique reflections merged from recorded 140979 ones (5.612° < 2θ < 151.542°) were used for structural analysis (R_{int} = 0.0241). Lattice parameters, *R*-factor on $F^2 > 2\sigma(F^2)$, weighted *R*-factor, goodness-of-fit, and Flack parameter (calculated from 10634 Parsons' quotients) are follows: *a* = 33.2238(3) Å, *b* = 14.44470(10) Å, *c* = 31.4133(2) Å, β = 101.5580(10)°, *V* = 14769.8(2) Å^3, *R* = 0.0602, *wR* = 0.1845, *S* = 1.072, χ = 0.193(8). Calculated density is 1.133. Linear absorption coefficient (μ) is 3.428. Residual electron density (max/min) is 0.45/–0.33 eÅ^{-3}. CCDC number 2243019.

The thermal ellipsoid plot of the asymmetric unit of **3**⊂CS is shown in Figure S3.3. One guest molecule was found in the asymmetric unit that is disordered with solvent *n*-hexane molecules. The occupancy of the guest is estimated as 35% so that its isotropic thermal parameters would have reasonable values (U_{iso} = 0.125–0.200), which was fixed in the refinement. Some restraints and constraints should be applied in refinement of a disordered model. The restraints used for the refinement are summarized in Figure S3.4. Information derived from NOESY correlations was used to refine the structure model of –CH_2–CH_2– bridge and –CH_2–O– bridge.

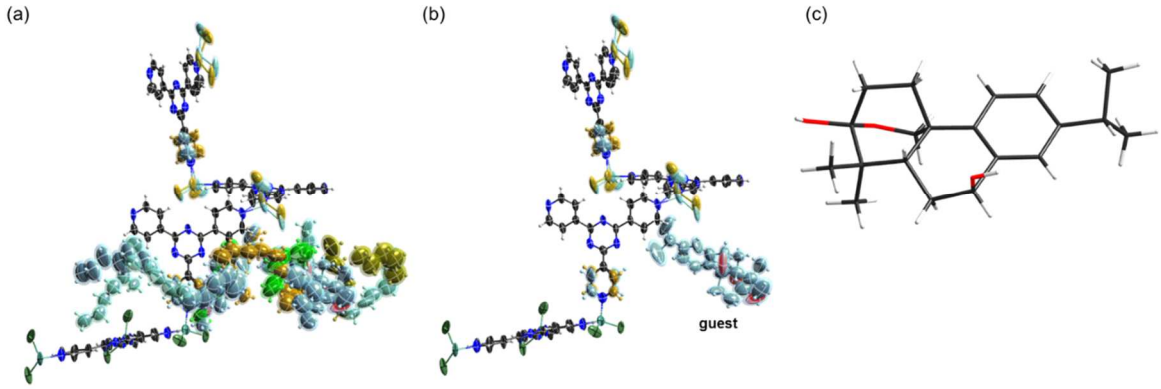

Supplementary Figure S3.3. Thermal ellipsoid plot at 50% probability in the asymmetric unit of **3**⊂CS. Enclosed atoms by the PART command in SHELXL were represented using the difference color code. Solvent molecules shown in (**a**) are omitted in (**b**) for clarity. Stick model of the guest is shown in (**c**).

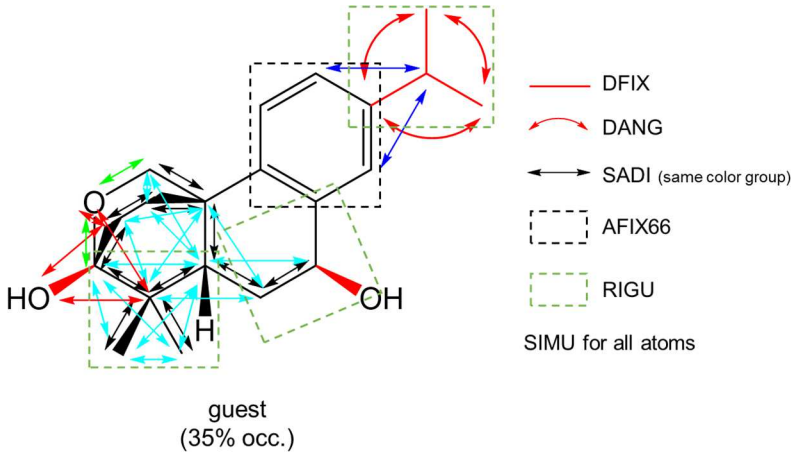

Supplementary Figure S3.4. Restraints and constraints applied in the refinement.

Crystallographic data for **4**

Crystal size: 60 × 20 × 10 μm^3, refined formula: $C_{20}H_{26}O_3$, formula weight (Mr) = 314.41, colorless needle, crystal system: Monoclinic, space group $P2_1$, Z = 2, 3327 unique reflections merged from recorded 15687 ones (9.744° < 2θ < 151.056°) were used for structural analysis (R_{int} = 0.0458). Lattice parameters, R-factor on $F^2 > 2\sigma(F^2)$, weighted R-factor, goodness-of-fit, and Flack parameter (calculated from 1290 Parsons' quotients) are follows: a = 5.9003(2) Å, b = 18.1536(8) Å, c = 7.7396(2) Å, β = 90.039(3)°, V = 829.00(5) Å^3, R = 0.0467, wR = 0.0980, S = 1.138, χ = −0.01(11). Calculated density is 1.260. Linear absorption coefficient (μ) is 0.658. Residual electron density (max/min) is 0.26/−0.17 eÅ^{-3}. CCDC number 2243020.

The thermal ellipsoid plot of **4** is shown in Figure S3.5.

Supplementary Figure S3.5. Thermal ellipsoid plot at 50% probability of **4**.

Crystallographic data for **5**⊂CS

Crystal size: 420 × 160 × 110 μm^3, refined formula: $C_{455.8}H_{414.8}Cl_{48}N_{96}O_{22.2}Zn_{24}$, formula weight (*Mr*) = 10862.89, colorless block, crystal system: Triclinic, space group *P*1, *Z* = 1, 111963 unique reflections merged from recorded 562314 ones (5.042° < 2θ < 151.448°) were used for structural analysis (R_{int} = 0.0293). Lattice parameters, *R*-factor on $F^2 > 2\sigma(F^2)$, weighted *R*-factor, goodness-of-fit, and Flack parameter (calculated from 32715 Parsons' quotients) are follows: *a* = 18.26360(10) Å, *b* = 27.3810(2) Å, *c* = 32.8700(2) Å, α = 68.1640(10)°, β = 77.8100(10)°, γ = 75.4920(10), *V* = 14643.8(3) Å^3, *R* = 0.0837, *wR* = 0.2695, *S* = 1.082, χ = 0.081(5). Calculated density is 1.232. Linear absorption coefficient (μ) is 3.517. Residual electron density (max/min) is 0.93/−0.52 eÅ^{-3}. CCDC number 2243021.

The thermal ellipsoid plot of the asymmetric unit of **5**⊂CS is shown in Figure S3.6. Inclusion of **5** leads to significant distortion of the host framework, resulting in space group change from achiral (*C*2/*c*) to chiral (*P*1). Sixteen guest molecules (A–P) were found in the asymmetric unit. The occupancies of four guest molecules (A, B, C, and D) are estimated as 100%, 100%, 35%, and 35%, respectively, so that their isotropic thermal parameters would have reasonable values (U_{iso} = 0.125–0.200), which was fixed in the refinement. Each of guests E, F, and G is disordered with solvent *n*-hexane, and their occupancies are estimated as 50%, 35%, and 35%, respectively, so that their isotropic thermal parameters would have reasonable values (U_{iso} = 0.125–0.200), which was fixed in the refinement. Two guest molecules (H and I) are overlapped on each other, and the guest H is further disordered with solvent *n*-hexane. The occupancies of the guests H and I are estimated as 60% and 40%, respectively, so that their isotropic thermal parameters would have reasonable values (U_{iso} = 0.125–0.200), which was fixed in the refinement. Two guest molecules (J and K) are overlapped on each other, and their occupancies are estimated as 50% and 50%, respectively, so that their isotropic thermal parameters would have reasonable values (U_{iso} = 0.125–0.200), which was fixed in the refinement. Two guest molecules (M and N) are overlapped on each other, and the guest M is further disordered with the guest L. The occupancies of the guests L, M, and N are estimated as 50%, 25%, and 25%, respectively, so that their isotropic thermal parameters would have reasonable values (U_{iso} = 0.125–0.200), which was fixed in the refinement. Two guest molecules (O and P) are overlapped on each other, and their occupancies are estimated as 25% and 25%, respectively, so that their isotropic thermal parameters would have reasonable values (U_{iso} = 0.125–0.200), which was fixed in the refinement. Some restraints should be applied in refinement of a disordered model. The restraints used for the refinement are summarized in Figure S3.7.

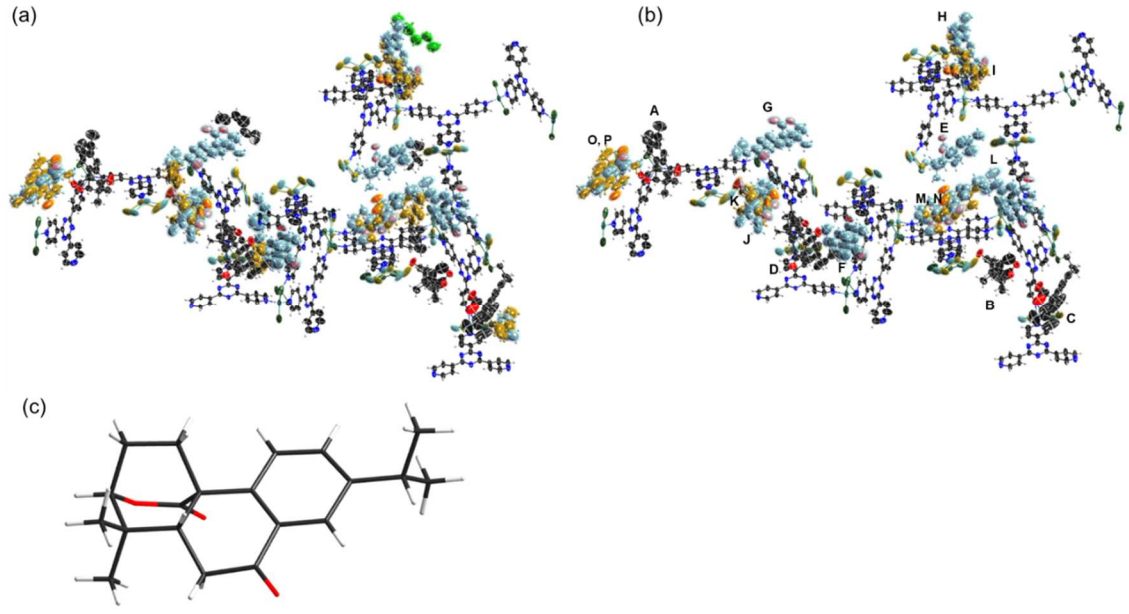

Supplementary Figure S3.6. Thermal ellipsoid plot at 50% probability in the asymmetric unit of **5**⊂CS. Enclosed atoms by the PART command in SHELXL were represented using the difference color code. Solvent molecules shown in (**a**) are omitted in (**b**) for clarity. Stick model of the guest A is shown in (**c**).

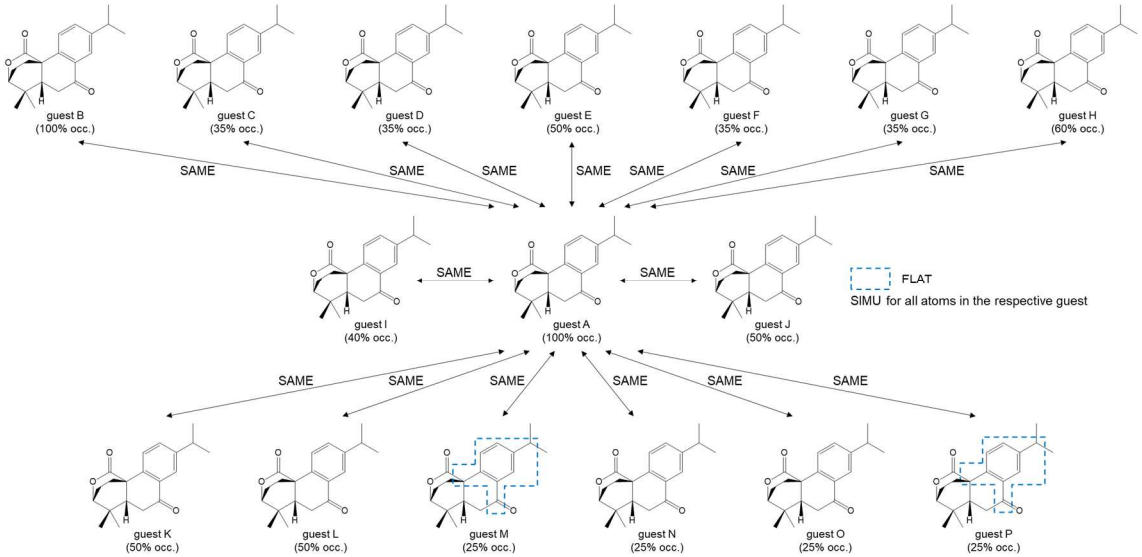

Supplementary Figure S3.7. Restraints applied in the refinement.

Crystallographic data for **6**⊂CS

Crystal size: 490 × 300 × 130 μm^3, refined formula: $C_{107.6}H_{107.9}Cl_{12}N_{24}O_3Zn_6$, formula weight (*Mr*) = 2602.89, colorless block, crystal system: Monoclinic, space group *C*2, *Z* = 4, 29940 unique reflections merged from recorded 142510 ones (5.688° < 2θ < 151.484°) were used for structural analysis (R_{int} = 0.0257). Lattice parameters, *R*-factor on $F^2 > 2\sigma(F^2)$, weighted *R*-factor, goodness-of-fit, and Flack parameter (calculated from 10662 Parsons' quotients) are follows: *a* = 33.1426(3) Å, *b* = 14.43210(10) Å, *c* = 31.7386(3) Å, β = 101.7090(10)°, *V* = 14865.2(2) Å^3, *R* = 0.0583, *wR* = 0.1860, *S* = 1.057, χ = 0.078(7). Calculated density is 1.163. Linear absorption coefficient (μ) is 3.429. Residual electron density (max/min) is 0.54/–0.46 eÅ^{-3}. CCDC number 2243022.

The thermal ellipsoid plot of the asymmetric unit of **6**⊂CS is shown in Figure S3.8. Three guest molecules (A, B, and C) were found in the asymmetric unit that are disordered with solvent *n*-hexane molecules. In addition, guests B and C are partially overlapped on each other. The occupancies of the guests A, B, and C are estimated as 50%, 50%, and 25%, respectively, so that their isotropic thermal parameters would have reasonable values (U_{iso} = 0.125–0.200), which was fixed in the refinement. Some restraints and constraints should be applied in refinement of a disordered model. A cyclohexanol ring in guest A shows two conformations of which occupancies are estimated as 29.1(11)% and 20.9(11)%, respectively, by least square refinement. Anisotropic atom displacement parameters of the corresponding atoms in two conformations were constrained using EADP command. Other restraints used for the refinement are summarized in Figure S3.9.

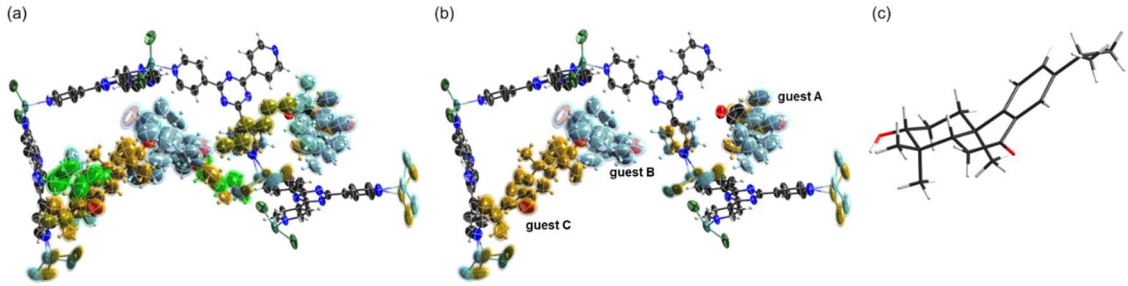

Supplementary Figure S3.8. Thermal ellipsoid plot at 50% probability in the asymmetric unit of **6**⊂CS. Enclosed atoms by the PART command in SHELXL were represented using the difference color code. Solvent molecules shown in (**a**) are omitted in (**b**) for clarity. Stick model of the guest A is shown in (**c**).

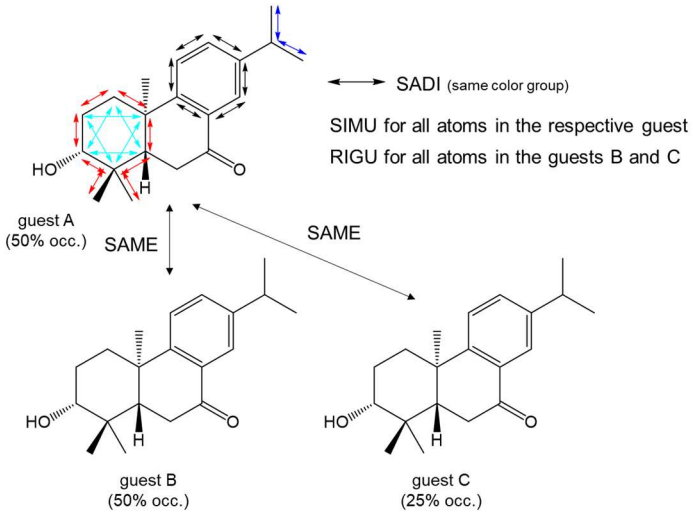

Supplementary Figure S3.9. Restraints applied in the refinement.

Crystallographic data for **7**⊂CS

Crystal size: 230 × 200 × 100 μm^3, refined formula: $C_{95.25}H_{89.85}Cl_{12}N_{24}O_{1.2}Zn_6$, formula weight (*Mr*) = 2407.58, colorless block, crystal system: Monoclinic, space group *C*2, *Z* = 4, 30085 unique reflections merged from recorded 143225 ones (5.42° < 2θ < 151.594°) were used for structural analysis (R_{int} = 0.0284). Lattice parameters, *R*-factor on $F^2 > 2\sigma(F^2)$, weighted *R*-factor, goodness-of-fit, and Flack parameter (calculated from 9968 Parsons' quotients) are follows: *a* = 33.4182(3) Å, *b* = 14.42860(10) Å, *c* = 31.7737(3) Å, β = 102.5810(10)°, *V* = 14952.7(2) Å^3, *R* = 0.0843, *wR* = 0.2565, *S* = 1.146, χ = 0.088(9). Calculated density is 1.069. Linear absorption coefficient (μ) is 3.364. Residual electron density (max/min) is 0.78/–0.65 eÅ^{-3}. CCDC number 2243023.

The thermal ellipsoid plot of the asymmetric unit of **7**⊂CS is shown in Figure S3.10. Two guest molecules (A and B) were found in the asymmetric unit that are partially overlapped on each other. The occupancies of the guests A and B are estimated as 40% and 20%, respectively, so that their isotropic thermal parameters would have reasonable values (U_{iso} = 0.125–0.200), which was fixed in the refinement. Some restraints should be applied in refinement of a disordered model. The restraints used for the refinement are summarized in Figure S3.11.

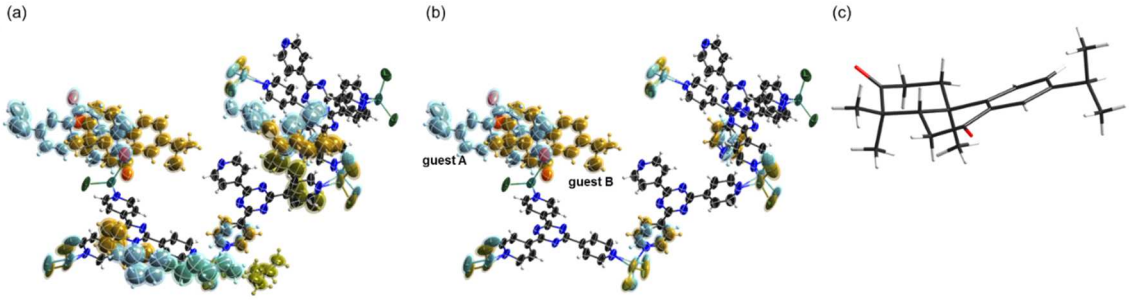

Supplementary Figure S3.10. Thermal ellipsoid plot at 50% probability in the asymmetric unit of **7**⊂CS. Enclosed atoms by the PART command in SHELXL were represented using the difference color code. Solvent molecules shown in (**a**) are omitted in (**b**) for clarity. Stick model of the guest A is shown in (**c**).

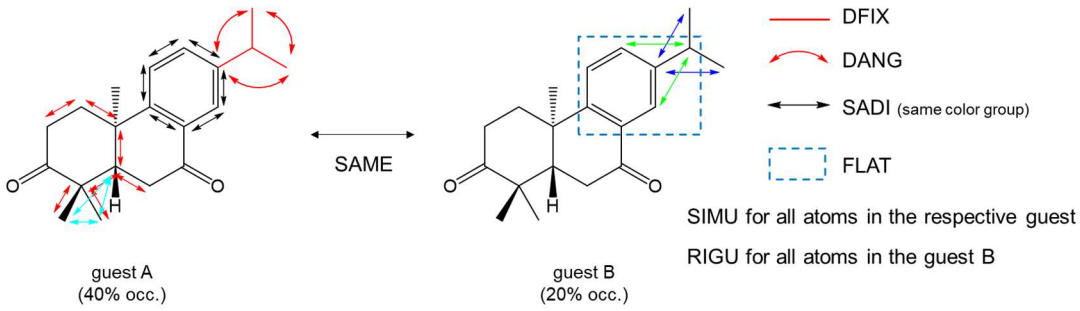

Supplementary Figure S3.11. Restraints applied in the refinement.

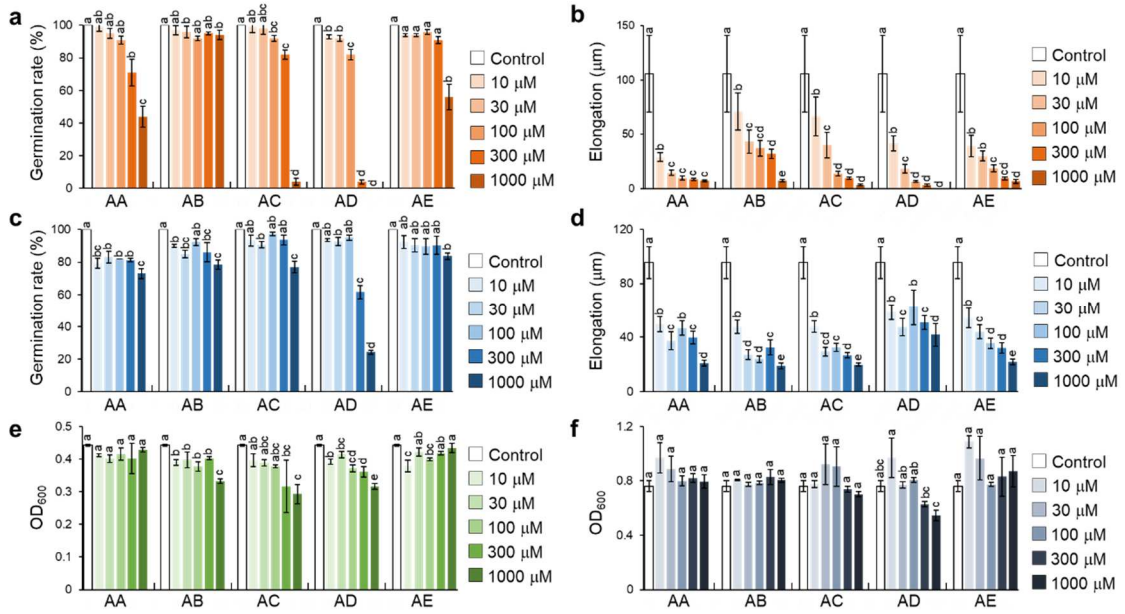

Supplementary Figure S3.12. Antimicrobial activities of abietoryzins A–E. (**a**) Effect of compounds on the germination of *Pyricularia oryzae*. Germination rates were determined 12 h after the treatment with compounds. (**b**) Effect of compounds on the conidial germ tube elongation of *P. oryzae*, which was measured 12 h after the treatment with compounds. (**c**) Effect of compounds on the germination of *Bipolaris oryzae*. Germination rates were determined 12 h after the treatment with the extracted compounds. (**d**) Effect of compounds on conidial germ tube elongation of *B. oryzae*, which was measured 12 h after the treatment with compounds. (**e**) Effect of compounds on the growth of *Burkholderia glumae*. Growth was assessed by measuring the OD_{600} at 21 h after the start of incubation. (**f**) Effect of compounds on the growth of *Xanthomonas oryzae* pv. *oryzae*. Growth was assessed by measuring OD_{600} 18 h after the start of incubation. AA: Abietoryzin A, AB: Abietoryzin B, AC: Abietoryzin C, AD: Abietoryzin D, AE: Abietoryzin E. Values and error bars are means ± standard deviation ($n = 3$). Different letters indicate significant differences ($p < 0.05$; Tukey-Kramer method).

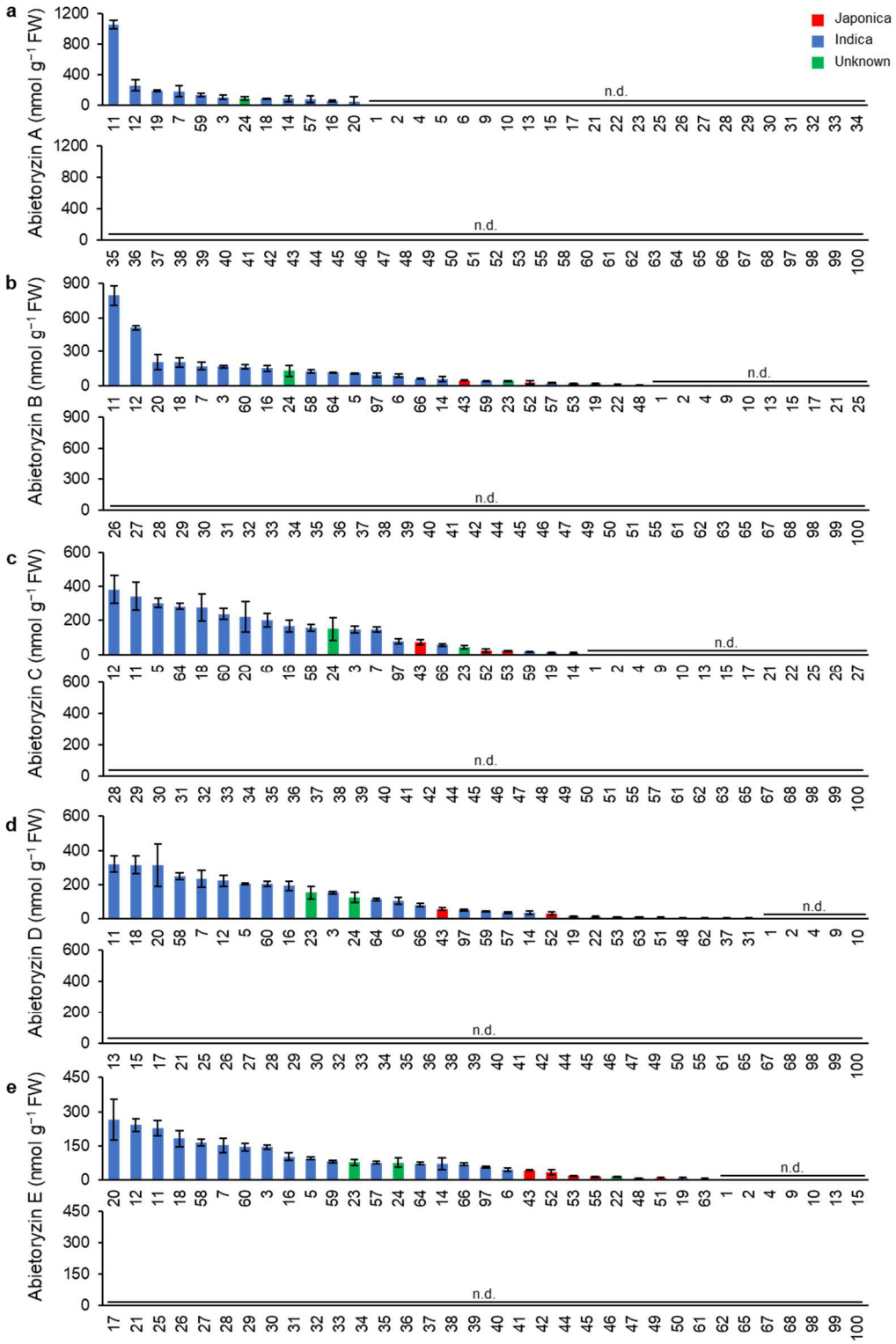

Supplementary Figure S3.13. Accumulation of Abietoryzins A–E (**a**–**e**) in WRC cultivars, respectively. Values are means ± SD of three biological replicates. n.d.: not detected.

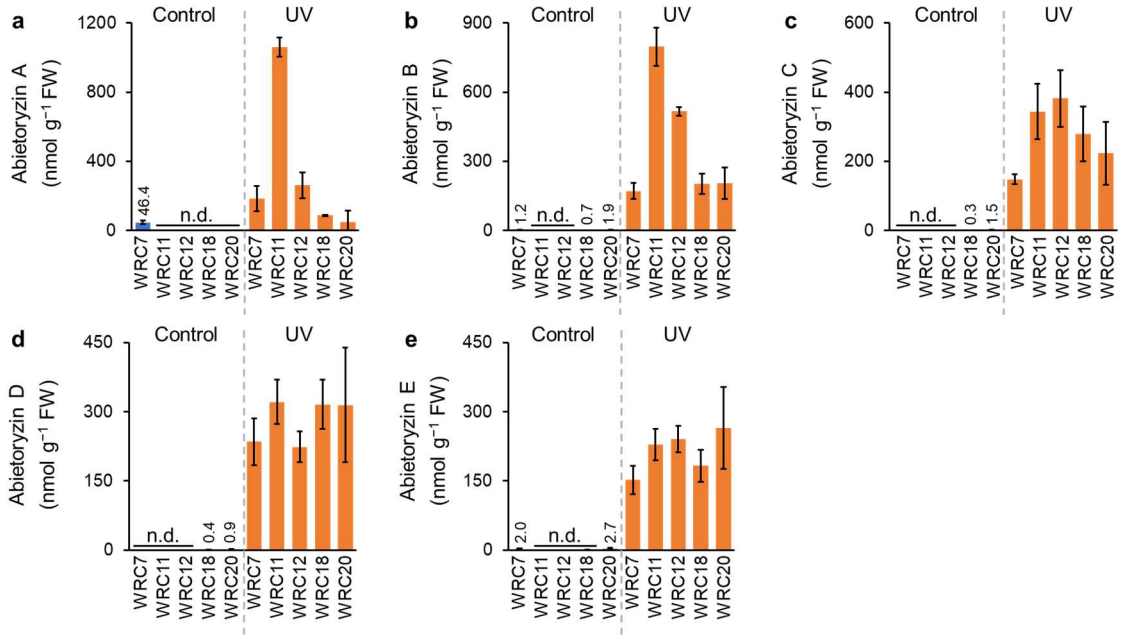

Supplementary Figure S3.14. Accumulation of abietoryzins A–E (**a**–**e**) in UV light-irradiated (UV) and unirradiated (control) leaves in the cultivars that accumulate abietoryzins at high concentrations. Values are means ± SD of three biological replicates. n.d.: not detected.

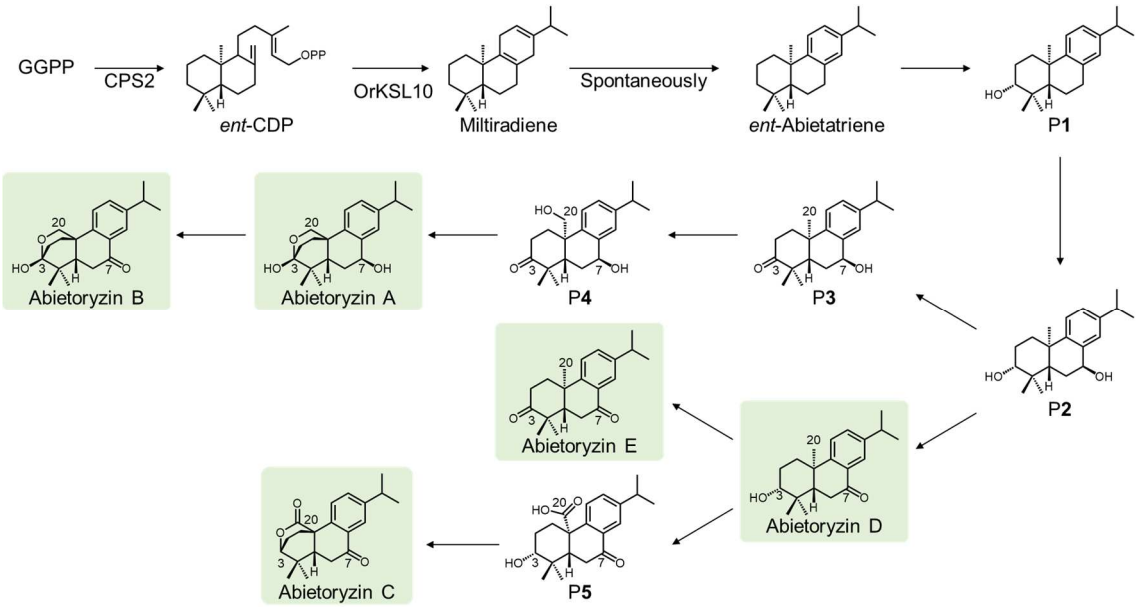

Supplementary Figure S3.15. Predicted biosynthesis pathway of abietoryzins A–E.

P1: 3-hydroxyabietatriene P2: 3,7-dihydroxyabietatriene P3: 7-hydroxyabietatriene-3-one P4: 7,20-dihydroxyabietatriene-3-one P5: 3-hydroxy-7-oxoabietatriene-20-calboxylic acid

Supplementary Table S3.1. ^{1}H NMR (600 MHz) spectroscopic data of abietoryzins D and E in $CDCl_3$.

Position	Abietoryzin D (**6**) ppm (multi; *J* in Hz)	Abietoryzin E (**7**) ppm (multi; *J* in Hz)
1α	2.37 (ddd; 13.2, 3.6, 3.6)	2.63 (ddd; 13.2, 6.6, 3.6)
1β	1.70 (ddd; 13.2, 13.2, 3.6)	2.02 (ddd; 13.2, 13.2, 5.4)
2α	1.79–1.91 (m; overlapped)	2.89 (ddd; 15.0, 13.2, 6.0)
2β	1.79–1.91 (m; overlapped)	2.55 (ddd; 15.6, 5.4, 3.6)
3	3.35 (dd; 11.4, 4.8)	–
5	1.79–1.91 (m; overlapped)	2.33 (dd; 13.8, 3.6)
6α	2.71 (d; 12.6)	2.81 (dd; 18.0, 13.8)
6β	2.73 (d; 4.8)	2.68 (dd; 18.0, 3.6)
11	7.26 (d; 8.4)	7.28 (d; 7.8)
12	7.40 (dd; 8.4, 2.4)	7.43 (dd; 7.8, 1.8)
14	7.87 (d; 2.4)	7.90 (d; 1.8)
15	2.92 (sept; 7.2)	2.94 (sept; 7.2)
16	1.242* (d; 7.2)	1.250* (d; 7.2)
17	1.246* (d; 7.2)	1.253* (d; 7.2)
18	0.97 (s)	1.20 (s)
19	1.05 (s)	1.14 (s)
20	1.240 (s)	1.44 (s)

* Assignments may be interchanged.

Supplementary Table S3.2. ^{13}C NMR (600 MHz) spectroscopic data of abietoryzins D and E in $CDCl_3$.

Position	Abietoryzin D (**6**)	Abietoryzin E (**7**)
	ppm	ppm
1	36.3[c]	37.5
2	27.6[b]	34.7
3	78.2	214.6
4	39.0	47.5
5	48.6	49.6
6	36.0[c]	36.5
7	199.6	198.5
8	130.6	130.6
9	153.0	133.0
10	37.7	37.0
11	124.0	124.3
12	132.7	151.3
13	147.1	147.6
14	125.0	125.3
15	33.7	33.8
16	23.9[a]	23.9[a]
17	23.8[a]	23.9[a]
18	15.0	25.1
19	27.7[b]	21.6
20	23.5[a]	22.9

*Assignments of the signals with the same letter may be interchanged.

Supplementary Table S3.3. Conditions of MRM and detection limits in LC-MS/MS analysis of phytoalexins.

Compound	Precursor ion (*m/z*)	Product ion (*m/z*)	Cone voltage (V)	Collision energy (eV)	Detection limit (nmol g^{-1} FW)
Abietoryzin A (**3**)	281.1	183.1	19	20	1.00
Abietoryzin B (**4**)	315.0	251.1	18	17	0.03
Abietoryzin C (**5**)	313.0	267.2	19	15	0.03
Abietoryzin D (**6**)	301.1	146.9	29	15	0.03
Abietoryzin E (**7**)	299.0	146.9	25	19	0.13

Supplementary Information. Spectroscopic analysis data for abietoyzins D (**6**) and E (**7**).

Abietoryzin D (**6**): CD spectra (Δε): –0.06 (298 nm), –0.50 (250 nm), –0.73 (225 nm) (50 μg mL^{-1}, ethanol); UV spectra (50 μg mL^{-1}, ethanol): λ_{max} nm (ε): 218 (7056), 252 (8160), and 301 (2142). $[\alpha]^{20}_{D}$=–30.1 (*c*=0.05, $CHCl_3$)

Abietoryzin E (**7**): CD spectra (Δε): –0.05 (298 nm), –0.50 (250 nm), –0.72 (225 nm) (50 μg mL^{-1}, ethanol); UV spectra (50 μg mL^{-1}, ethanol): λ_{max} nm (ε): 213 (6204), 252 (4464), and 300 (864). $[\alpha]^{20}_{D}$=–43.1 (*c*=0.05, $CHCl_3$)